UNIVERSIDADE FEDERAL DO PARANÁ

GUSTAVO MACHADO MARANGON

GÊNESE E EVOLUÇÃO DE MICROBIALITOS LACUSTRES QUATERNÁRIOS DO EXTREMO SUL DA PATAGÔNIA CHILENA: ESTUDO DE MORFOLOGIA, FÁBRICA, MINERALOGIA E GEOQUÍMICA

CURITIBA

2022

GUSTAVO MACHADO MARANGON

GÊNESE E EVOLUÇÃO DE MICROBIALITOS LACUSTRES QUATERNÁRIOS DO EXTREMO SUL DA PATAGÔNIA CHILENA: ESTUDO DE MORFOLOGIA, FÁBRICA, MINERALOGIA E GEOQUÍMICA

Dissertação apresentada ao Programa de Pós-graduação em Geologia, Setor de Ciências da Terra, Universidade Federal do Paraná.

Orientador: Prof. Dr. Leonardo Fadel Cury

CURITIBA

2022

Catalogação na Fonte: Sistema de Bibliotecas, UFPR
Biblioteca de Ciência e Tecnologia

M311g

Marangon, Gustavo Machado
Gênese e evolução de microbialitos lacustres quaternários do extremo sul da Patagônia Chilena: estudo de morfologia, fábrica, mineralogia e geoquímica [recurso eletrônico] / Gustavo Machado Marangon. – Curitiba, 2022.

Dissertação - Universidade Federal do Paraná, Setor de Ciências da Terra, Programa de Pós-Graduação em Geologia, 2022.

Orientador: Leonardo Fadel Cury .

1. Sedimentalogia. 2. Carbonatos. 3. Isótopos estáveis. 4. Trombólitos. 5. Microbialitos. I. Universidade Federal do Paraná. II. Cury, Leonardo Fadel. III. . Título.

CDD: 551.304

Bibliotecário: Elias Barbosa da Silva CRB-9/1894

TERMO DE APROVAÇÃO

Os membros da Banca Examinadora designada pelo Colegiado do Programa de Pós-Graduação GEOLOGIA da Universidade Federal do Paraná foram convocados para realizar a arguição da Dissertação de Mestrado de **GUSTAVO MACHADO MARANGON** intitulada: **GÊNESE E EVOLUÇÃO DE MICROBIALITOS LACUSTRES QUATERNÁRIOS DO EXTREMO SUL DA PATAGÔNIA CHILENA: ESTUDO DE MORFOLOGIA, FÁBRICA, MINERALOGIA E GEOQUÍMICA**, sob orientação do Prof. Dr. LEONARDO FADEL CURY, que após terem inquirido o aluno e realizada a avaliação do trabalho, são de parecer pela sua APROVAÇÃO no rito de defesa.

A outorga do título de mestre está sujeita à homologação pelo colegiado, ao atendimento de todas as indicações e correções solicitadas pela banca e ao pleno atendimento das demandas regimentais do Programa de Pós-Graduação.

CURITIBA, 25 de Fevereiro de 2022.

Assinatura Eletrônica
03/03/2022 16:25:38.0
LEONARDO FADEL CURY
Presidente da Banca Examinadora

Assinatura Eletrônica
02/03/2022 13:28:17.0
DANIEL ARIZTEGUI
Avaliador Externo (UNIVERSIDADE DE GENEBRA)

Assinatura Eletrônica
11/03/2022 23:25:46.0
CRISOGONO DE OLIVEIRA VASCONCELOS
Avaliador Externo (INSTITUTO FEDERAL DE TECNOLOGIA DE ZURIQUE)

AGRADECIMENTOS

Ao meu orientador e amigo prof. Dr. Leonardo Fadel Cury, pela confiança, apoio e solicitude durante este trabalho. Ao professor Maurício Calderón, da *Universidad Andrés Bello*, aos estudantes e geólogos Gustavo Barrientos, Paulo Quezada, Valeria Molina e Vicente Amand pelo companheirismo e auxílio no trabalho de campo. Ao professor Edenilson do Nascimento (UFPR) pelo auxílio na preparação para o campo e companheirismo durante o mesmo. Ao professor Gustavo Athayde Barbosa pelo auxílio e companheirismo em campo e posterior realização das análises físico-químicas de água junto ao Laboratório de Pesquisas Hidrogeológicas (UFPR).

Ao Instituto LAMIR (UFPR), pela recepção e fornecimento de todo tipo de suporte necessário para realização do trabalho laboratorial. Em especial aos técnicos, Diego Portela Fernandes, Flávia Priscila Afonso, Joicy Micheletto, Leandro Keiji e Shirley Santos Cezar, pela preparação de amostras, realização de análises e discussões metodológicas. À professora Dra. Anelize Bahniuk pela solicitude e ajuda na preparação e interpretação de dados petrográficos e geoquímicos. Aos colegas Carolina Valenzuela, Guilherme Fedalto, Joana Rosin, Tatiana Stepanenko e Larissa Santos pelas discussões geológicas e metodológicas.

A Shell/FUNPAR, através do projeto '*Diagenesis:* Diagênese nas sequências carbonáticas do Pré-Sal e seu impacto na exploração e produção de reservatórios de hidrocarbonetos' (processo nº 23075.193990/2017-07), pelo financiamento da bolsa de pesquisa e investimento na estrutura necessária para realização do trabalho.

Agradeço a todos aqueles que estiveram ao meu lado nestes difíceis tempos de COVID-19, em especial meus pais, Rosane e Roberto, por toda a força. Aos pesquisadores brasileiros comprometidos com seu povo e com os métodos de suas respectivas ciências, que resistem a esses tempos de obscuridade e negacionismo científico.

RESUMO

Este estudo nos microbialitos sub-fósseis da *Laguna del Toro* (inédito), no extremo sul da Patagônia, demonstra como a investigação em múltipla-escala de microbialitos, aliada ao uso de isótopos de oxigênio e carbono, podem fornecer ideias de como os microbialitos registram as variantes intrínsecas e extrínsecas de seu crescimento e litificação carbonática. Os depósitos são extensos pavimentos de estruturas em domo (0,1 – 1,5 m), localmente sobrepostos por pináculos (1,5 – 3 m). Ambos apresentam mesoestrutura de trombólitos, com estrutura interna composta por complexa assembleia de microfábricas micríticas e microesparíticas. Domínios micríticos são formados por bolsões de micrita maciça e peloidal interconectados por lâminas micríticas. Esses estão em contato com domínios microesparíticos que são, frequentemente, cortados por micrita em *clots*. As fábricas de micrita castanho-escura são compostas de nanoesferas de Mg-Ca-carbonato agregadas formando poliedros triangulares, permeados por feições mucosas e em forma de colmeia, fósseis de substâncias polímeras extracelulares (EPS). Essas feições envolvem filamentos achatados e tubulares de cianobactérias, com 15 a 175 µm de comprimento. A fábrica microesparítica é composta de cristais límpidos e euédricos com forma de poliedros triangulares e romboedros, com tamanhos entre 12 - 20 µm. Amostras de micrita coletadas por *micro-drill,* são relativamente enriquecidas em ^{13}C (3.02 - 4.69‰ VPDB), enquanto o sinal isotópico da microesparita é relativamente mais leve (3.36 - 3.81‰ VPDB). As microfábricas juntamente com os sinais isotópicos sugerem que a micrita fora formada por mineralização precoce do EPS, via captura de CO_2 pela fotossíntese de cianobactérias, e consequente aumento de alcalinidade. A microesparita, por outro lado, é interpretada como associada à degradação dos domínios do EPS ricos em cianobactérias e subsequente calcificação. As fábricas difusas, como a micrita em *clots*, podem ter sido formadas pela diminuição de tais domínios, possivelmente pela ação de bactérias heterotróficas ou processos físico-químicos. A mudança nos estilos de crescimento da comunidade microbiana (refletidos nas macroestruturas), dos mounds para os pináculos, é mais provavelmente associada a mudanças ambientais no paleolago do que mudanças internas na comunidade-microbiana. A identificação de estruturas microbianas em rochas carbonáticas do registro geológico pode ser um trabalho difícil, visto que os diversos processos diagenéticos obliteram as bioestruturas. Neste sentido, os microbialitos da *Laguna del Toro* podem fornecer informações sobre como as microfábricas e morfologia dos depósitos, tipicamente encontradas no registro geológico, gravam os fatores internos (escala microbiana) e externos (paleoambiente) de precipitação de carbonatos em comunidades microbianas. Podendo, assim, serem utilizados como análogos para estudos de carbonatos do registro geológico.

Palavras-chave: Trombólitos; Microfábricas; Sedimentologia; Precipitação carbonática; Isótopos estáveis.

ABSTRACT

This study on the sub-fossil microbialites within Laguna del Toro (unpublished publication), southernmost Patagonia, shows how the microbialite multi-scale investigation allied with carbonate carbon and oxygen stable isotopes can provide insights on how microbialites registries the biological (intrinsic) and environmental (extrinsic) conditionings on carbonate precipitation within microbial communities. The deposits are extensive beds of mounds in the lake margins, covered by clusters of m-height pinnacles. Both show thrombolite mesostructure, which is internally composed of a complex assemblage of micritic and microsparitic microfabrics. Domains of interconnected pockets of massive, peloidal, and microlaminated dark micrite are bounded by microsparite. The latter is often crosscut by clotted micrite and structureless mixed micrite and microsparite. The dark micritic domains are formed by subhedral triangular polyhedrons aggregates of Mg-Ca-nanospheres, permeated by mucous-like and honeycomb-like fossilized EPS. The mucous-like features are locally embedding flattened or tubular hollow filamentous cyanobacteria, with 15 to 175 µm long. Microsparite fabrics is composed of limpid, euhedral triangular polyhedrons and rhombohedrons of calcite, with 12 to 20 µm wide. Micrite micro-drilled samples are enriched in ^{13}C (3.02 - 4.69‰ VPDB) and microsparite is lighter (3.36 - 3.81‰ VPDB). Microfabrics and isotopic data suggest that the large micritic domains are formed by early EPS mineralization via photosynthetic CO_2 uptake and alkalinity enhancement. Microsparite, otherwise, is interpreted to be associated with degradation of the cyanobacteria-rich biofilms and physiochemical precipitation. Diffuse fabrics (*e.g.*, Clotted micrite) could have been formed by the shrinkage of these cyanobacterial domains, possibly due to heterotrophic or physiochemical processes. The change in microbial-community growth morphology, from mounds to pinnacles, is due to paleolacustrine environmental shifts rather than internal microbial-community modification. It is often difficult to understand the genesis of microbialite structures in the geologic record, because of their lack of biostructures preservation. In this way, this study may serve as an analog to diagnosing and interpreting microbialite structures in ancient carbonate rocks.

Keywords: Thrombolite; Microfabrics; Sedimentology; Carbonate precipitation; Stable isotopes.

LISTA DE FIGURAS

ARTIGO: SUB-FOSSIL LACUSTRINE MICROBIALITE PINNACLES: BUILD-UP FORMATION AT LAGUNA DEL TORO, SOUTHERNMOST PATAGONIA

LISTA DE TABELAS

SUMÁRIO

1 INTRODUÇÃO

Microbialitos são depósitos organossedimentares formadas por diversos processos de precipitação de carbonatos associados à atividade metabólica em comunidades microbianas e *trapping and binding* de grãos detríticos (Burne e Moore, 1987; Riding, 2011a). Os primeiros trabalhos que reportaram depósitos organossedimentares se referiam a rochas com estrutura laminada, os estromatólitos (*e.g.*, Kalkowsky, 1908; Golubic e Hoffman, 1976). Essas rochas são os registros mais antigos de vida na Terra, no Arqueano (Hoffman *et al.*, 1999), e sua ocorrência é identificada em 85% da história do Planeta Terra (Grotzinger e Knoll, 1999). Tendo sua ocorrência distribuída por diversos ambientes marinhos e continentais (Riding, 2011b). A partir do trabalho de Aitken (1967), quando os trombólitos foram definidos, diversos estudos passaram a reportar depósitos não-laminados como também sendo organossedimentares, e a identificação da ocorrência destes no registro geológico passou a se expandir (*e.g.*, Pratt e James, 1982; Walter e Heyes, 1985; Kennard e James, 1986; Guo e Riding, 1992; Kahle, 2001; Harwood e Sumner, 2012; Bosence e Gallois, 2021).

Com a identificação destas rochas, passou-se a perceber que a partir do Neoproterozóico houve uma mudança na morfologia dos microbialitos (Awramik, 1971; Aitken e Narbonne,1989). Neste período, diminuiu a ocorrência dos estromatólitos enquanto expandia a ocorrência de rochas não-laminadas nos ambientes antes ocupados por aqueles. Tal expansão é registrada até o fim do Cambriano, no entanto, os microbialitos não-laminados são encontrados em diversos paleoambientes do Paleozóico ao Quaternário, onde ocorrem principalmente em lagos (Kennard e James, 1986; Shapiro e Awaramik, 2000; Shapiro, 2004; Dupraz *et al.*, 2011). Estas diferentes estruturas ocorrendo de modo diversificado ao longo do tempo, devem representar diferentes processos de litificação e também mudanças paleoclimáticas significativas (Dupraz *et al.*, 2011; Harwood e Sumner, 2012; Suarez-Gonzalez *et al.*, 2019).

As feições distintivas dos microbialitos não-laminados, em especial os trombólitos, são os *mesoclots* (*sensu* Shapiro, 2000), a micrita em *clots* e a micrita peloidal (Fig. 1; Aitken, 1967; Kennard e James, 1986; Shapiro, 2000). As primeiras são meso-estruturas caracterizadas por carbonatos com formas irregulares circundados por poros ou sedimentos (Aitken, 1967; Shapiro, 2000). As últimas são

microestruturas que formam o interior dos *mesoclots* (Kennard e James, 1986; Shapiro, 2000). Diversos estudos com esteiras microbianas vivas propuseram processos de formação de feições não-laminadas (e.g. Riding *et al.*, 1991; Arp *et al.*, 2003; Dupraz *et al.*, 2004; Dupraz *et al.*, 2009; Burne *et al.*, 2014; Theisen *et al.*, 2015; Bischoff *et al.*, 2020). Embora esses estudos forneçam informações primordiais para entender a gênese de tais estruturas, muitas vezes é difícil reconhecer as mesmas feições das esteiras vivas nas rochas do registro. Uma vez que os análogos *in-vivo* utilizados não passaram por litificação total, portanto, por significativa mineralização, degradação da matéria orgânica e alteração diagenética.

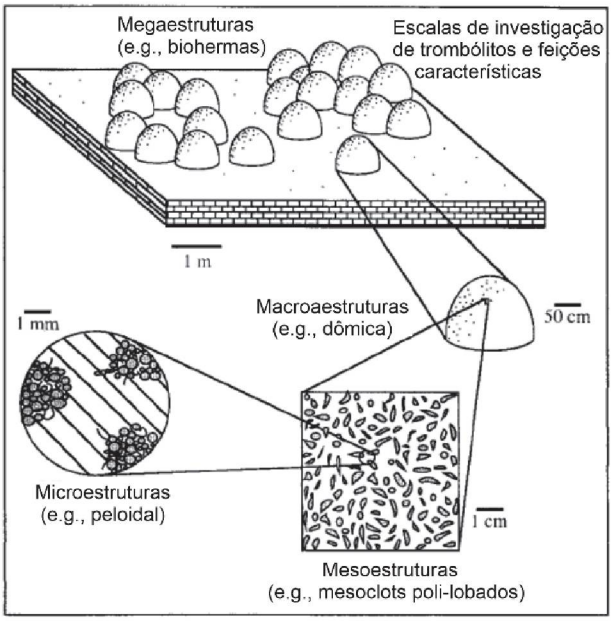

Figura 1 - Escalas de investigação geológica e feições distintivas dos trombólitos. Adaptado de Shapiro (2000).

O lago alcalino *Laguna del Toro*, no extremo sul da Patagônia Chilena, apresenta extensos depósitos de trombólitos sub-fósseis (inédito). Extensas camadas de estruturas dômicas e, mais localizadamente, pináculos estão depositados nas margens do lago. O fato dos microbialitos estarem plenamente litificados, com estruturas primárias petrograficamente bem preservadas e apresentarem morfologias únicas; além da possibilidade de visualizar elementos, ainda presentes, do paleoambiente lacustre, tornam a localidade única para o estudo em múltipla escala de estruturas microbialíticas não-laminadas.

Esta dissertação reporta, portanto, os estudos feitos a respeito da gênese dos microbialitos quaternários da *Laguna del Toro*. É, ainda, uma tentativa de prover informações sobre os possíveis fatores intrínsecos e extrínsecos de precipitação em comunidades microbianas (*sensu* Dupraz e Visscher, 2005) e como estes podem

controlar a morfologia, estrutura interna e microfábrica de trombólitos. Com a investigação em múltipla-escala (Fig. 1) podemos identificar como os processos biológicos estão registrados nas diferentes escalas de estruturas. Além disso, como que o ambiente externo à comunidade microbiana pode ter controlado as distintas feições dos microbialitos. Logo, pode-se utilizar este estudo como análogo para investigações petrográficas e sedimentológicas de rochas carbonáticas do registro geológico.

2 LOCALIZAÇÃO E CONTEXTO GEOGRÁFICO-GEOLÓGICO

Localizada 50 km a leste do orógeno andino, a *Laguna del Toro* é um pequeno lago endorreico (15 km²), nas margens nordeste do *Seno Otway* e noroeste do Estreito de Magalhães (Fig. 1). A localidade está no extremo sul da patagônia, região de *Magallanes y Antartica Chilena*, Chile. Nesta região do planeta, as correntes circumpolares antárticas chegam no continente sul-americano, vindas do pacífico, e se chocam com a cordilheira dos andes austrais forçando a precipitação orográfica (Carrasco *et al.*, 2002). Isto faz com que toda região de Magalhães se encontre em uma zona de sombra de chuvas, caracterizada por um clima continental frio transicional de sub-úmido para semi-árido com vegetações de estepes (Coronato, 2008).

Distante do cinturão orogênico, o lago se encontra sobre a bacia de antepaís de *Magallanes* (Fig. 1A). Esta bacia tem sua formação após o fechamento da bacia de *back-arc* de *Rocas Verdes*, no Cretáceo Superior (Fosdick *et al.*, 2011). Ali se instalou um ambiente marinho profundo, com máxima inundação no Conaciano-Campaniano (Fildani *et al.*, 2008). A partir de então, registra-se a continentalização da bacia, marcadamente no Mioceno, com a deposição fluvial da Formação *Santa-Cruz* (Ramos, 1989) e de sua correlata, a Formação *Palomares* (González, 1965), aflorante nas margens da Laguna del Toro. A partir de 18 Ma, a região passa a experimentar uma tectônica extensional, associada à subducção da dorsal assísmica do chile e da formação de janela astenosférica sob a patagônia (Breitsprecher e Thorkelson, 2009). Durante o Cenozóico, portanto, se instalaram sistemas de riftes de direção NE-SW, ortogonais ao orógeno, que levaram à formação do Estreito de Magalhães (Diraison *et al.*, 1997; Diraison *et al.*, 2000; Ghiglione *et al.*, 2012). Junto a isso, campos vulcânicos alcalinos se instalaram no retroarco, como o campo vulcânico de *Pali Aike* (Ramos e Kay, 1992), que teve intensa atividade durante o Plioceno-Holoceno

(Mazzarini e Orazio, 2003). Este campo está marcado na paisagem por extenso platô basáltico à 80 km da *Laguna del Toro* (Fig. 1B).

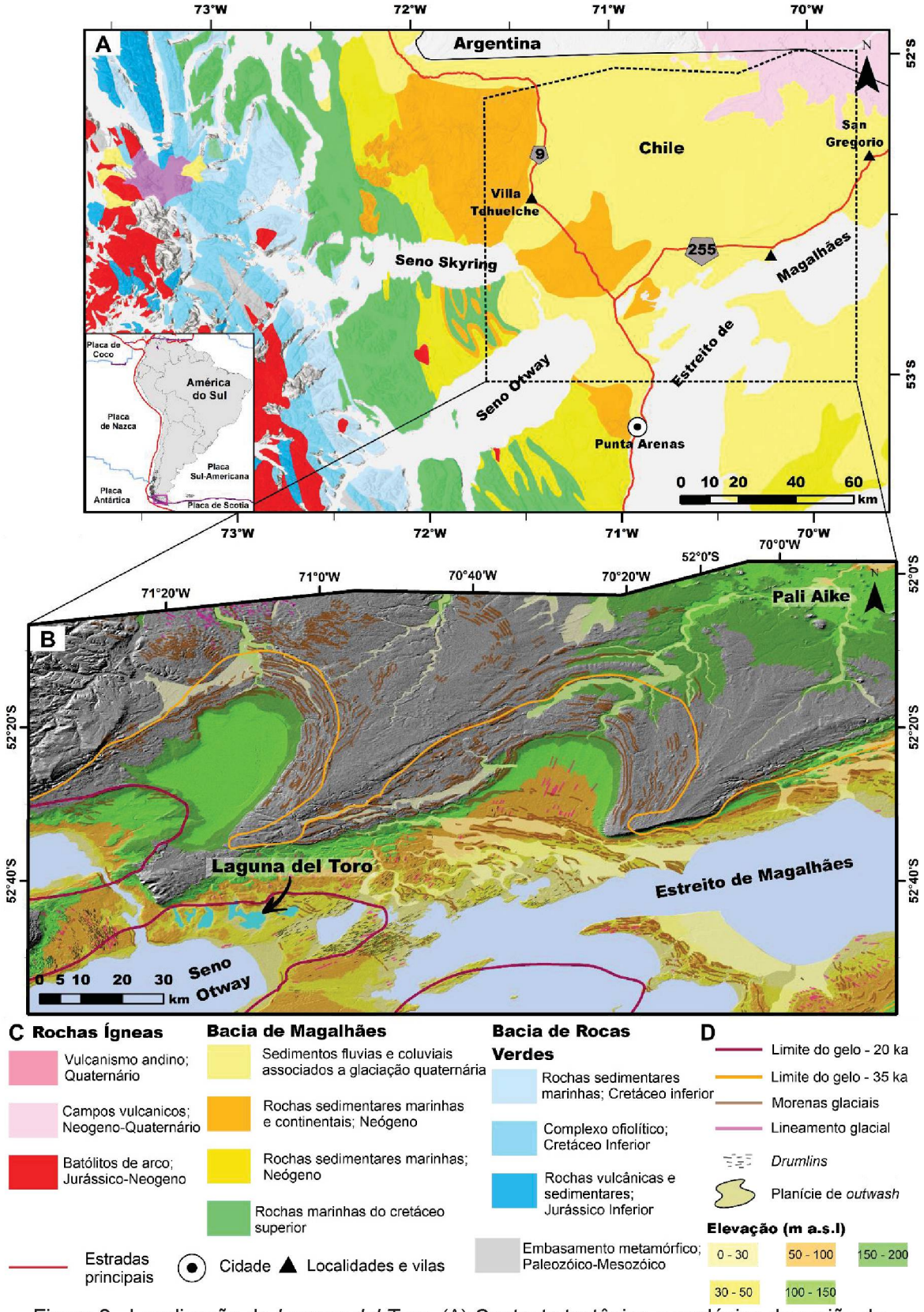

Figura 2 - Localização da *Laguna del Toro*. (A) Contexto tectônico e geológico da região de Magalhães. (B) Mapa de altitudes sobre relevo sombreado da região *da Laguna del Toro*, com feições paleoglaciais associadas. (C) legenda de 'A'. (D) Legenda de 'B'.

Durante o Plioceno e Pleistoceno a sedimentação e modelagem morfológica da região do Estreito de Magalhães esteve associada às flutuações do Campo de Gelo da Patagônia (CGP; Fig. 1B). As geleiras de altitude passaram a ocupar áreas da planície no antepaís, durante o último período glacial, que teve seu máximo local há 47 ka (Davies *et al.*, 2020). Neste período, lobos glaciares de direção NE-SW ocupavam vastas áreas de baixa altitude (Killian *et al.*, 2013). Há cerca de 20 ka inicia-se a deglaciação local e formação de grandes lagos proglaciais (McCulloch *et al.*, 2005), que tiveram seu máximo de extensão em 15 ka (Davies *et al.*, 2020). Com a abertura da conexão com o Oceano Pacífico, os paleolagos foram drenados. Restando uma região de baixa altitude submersa, aonde estão os *Seno Skyring* e *Otway* e suas prolongações emersas com diversas feições de erosão glacial e depósitos glaciais (Clapperton *et al.*, 1995; McCulloch e Bentley, 1998; Davies *et al.*, 2020).

A *Laguna del Toro* está sobre depósitos conglomeráticos associados às flutuações glaciais quaternárias. Sua gênese e evolução limnológica, no entanto, são desconhecidas, uma vez que não foi encontrada nenhum tipo de bibliografia sobre o lago e vizinhanças.

3 MATERIAIS E MÉTODOS

A caracterização preliminar físico-química da água da *Laguna del Toro* foi realizada visando comparar com as possíveis condições pretéritas de precipitação dos carbonatos. Em etapa de preparação para o trabalho de campo, aspectos geométricos (eixo, largura e etc.) e de regime hídrico (canais afluentes e efluentes) foram medidos e descritos através do *Google Earth*. Os parâmetros físico-químicos de água, medidos *in-situ* (pH, temperatura, sais totais dissolvidos e condutividade), foram aferidos em seis localidades pelo Professor Gustavo Athayde Barbosa, utilizando um multiparâmetro Horiba. O mesmo coletou duas amostras do lago e uma de drenagem afluente para caracterização hidroquímica (Fig. 3). Esta ocorreu por diversas análises conduzidas pelo Professor e equipe do Laboratório de Pesquisas Hidrogeológicas da Universidade Federal do Paraná (LPH-UFPR), que nos cederam os dados. Estes foram, então, caracterizados a partir do diagrama de Piper, através do programa *EasyQuim*. Os indicies de saturação dos minerais foram calculados no software PHREEQC (Parkhurst *et al.*, 1982).

Em campo foram percorridas todas as margens a norte até a margem sudeste do lago (em sentido horário, Fig. 3), onde foram descritos os depósitos carbonáticos e siliciclásticos associados. Os pontos foram nomeados “TOR”, seguido do número da mesorregião do lago (I, II, III e etc.; Fig. 3). A macro e mesoestrutura dos depósitos carbonáticos foram descritas e amostras foram coletadas, sendo nomeadas com letras segundo o ponto (p. ex., TOR IV A, B e etc.). Resultando em 28 amostras de mão e 60 amostras em pó de carbonatos que se somaram a 14 e 35, respectivamente, anteriormente coletadas por equipe do instituto LAMIR (UFPR). As amostras em pó foram coletadas por ferramenta elétrica de perfuração com broca vídea. Esta amostragem foi feita em cinco microbialitos com morfologia em pináculo selecionados em diferentes margens do lago. Cerca de 2 g de amostra foram coletadas a cada 10 cm ao longo do eixo vertical do pináculo.

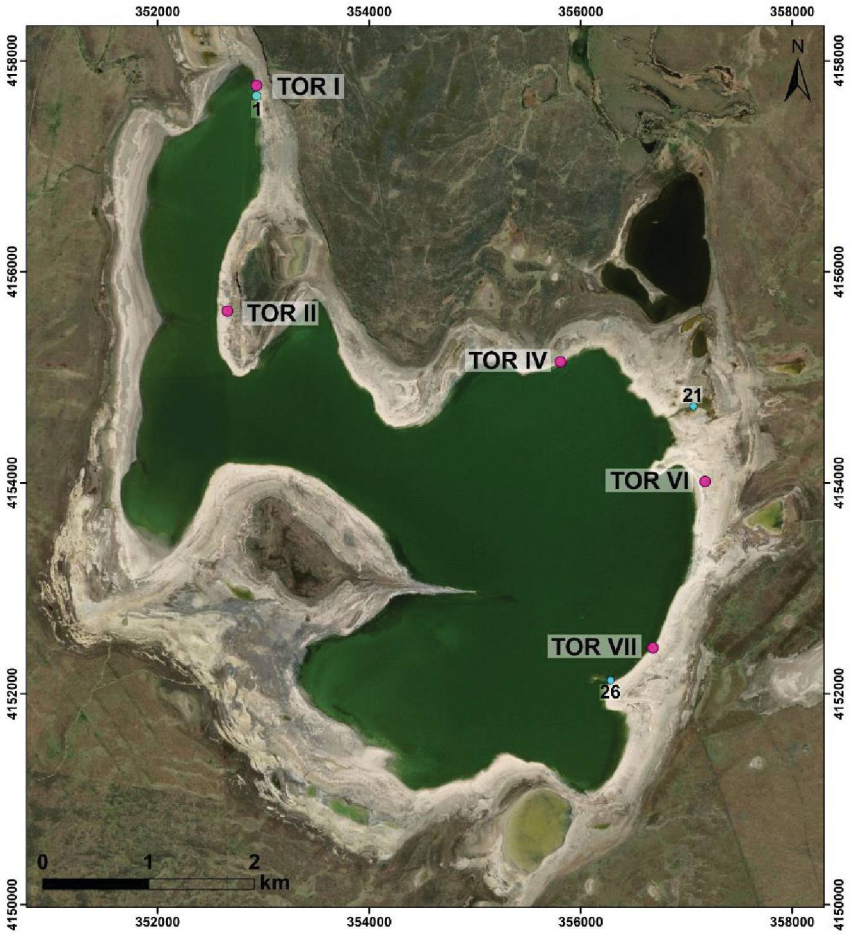

Figura 3 - Imagem de satélite da Laguna del Toro, com pontos de amostragem de rocha (pontos rosas) e água (pontos azuis).

As amostras de mão foram utilizadas para confecção de 37 lâminas delgadas coloridas com alizarina (para diferenciação de calcita e dolomita), que foram descritas em microscópio de luz transmitida para caracterização de microfábrica. Após a

petrografia, duas lâminas delgadas e cerca de 10 fragmentos de rocha foram impregnadas por Au-Pd, para análise em microscópio eletrônico de varredura (MEV), modelo JEOL 6010LA. Tal análise visou identificar aspectos texturais e microestruturais de cada microfábrica previamente identificada. Foi utilizado ainda um equipamento acoplado de espectroscopia por energia dispersiva (MEV-EDS), modelo JEOL EX-94410T1L11, como recurso na identificação de fases minerais (Apêndice 1). Com o qual ainda foi possível fazer mapas elementais (Apêndice 2). A aceleração voltaica para descrição textural foi entre 3 e 10 keV e para as análises de EDS de 20 keV, com distanciamento de 9 a 14 mm.

Junto ao MEV-EDS, foram realizadas 36 análises de difratometria de raios-X (DRX) para caracterização mineralógica de rocha total dos microbialitos (Apêndice 3). Para isto foram utilizadas amostras coletadas em campo na forma de pó e amostras de mão, que passaram por moagem em almofariz de ágata. Estas foram analisadas em equipamento *Malvern PANalytical Empyrean*, com tubo de raios-X de configuração 2θ (gerador-detector), de cobre Kα λ=1,54060 Å, e detector *XCELERATOR* (ângulo mínimo de 0,0001°). Os difratogramas resultantes foram analisados e processados no programa *High Score* da *PANanalytical*.

Para melhor identificar e diferenciar os distintos processos que levaram à precipitação carbonática foram utilizadas amostras em pó dos pináculos e amostras de mão dos pináculos e *mounds* (estruturas dômicas). A partir de dez fatias de rochas, foram coletadas amostras, utilizando *microdrill*, das microfábricas puramente micríticas, puramente microesparíticas e misturadas (micrita em *clots*). Resultando, portanto, em 114 amostras de rocha-total de pináculos, 3 de rocha-total de *mounds* e 21 sub-amostras de micro-fábricas (Apêndices 4, 5).

As razões isotópicas foram determinadas utilizando a técnica de *Gas-Bench II*, em um Espectrometro de Massas de Razão Isotópica (IRMS), modelo *Thermo Fischer Delta V Advantage*. A liberação de CO2 das amostras foi obtida através da digestão dos carbonatos, utilizando um ácido ortofosfórico, à 72ºC. Os resultados das razões isotópicas dos carbonatos estão reportados em desvio per mil (‰), referenciados ao VPDB (*Vienna Pee Dee Belemnite*).

4 RESULTADOS E DISCUSSÕES

Os resultados e as discussões deste trabalho serão apresentados na forma de artigo científico a ser submetido em revista de relevância internacional.

SUB-FOSSIL LACUSTRINE MICROBIALITE PINNACLES: BUILD-UP FORMATION AT LAGUNA DEL TORO, SOUTHERNMOST PATAGONIA

ABSTRACT

This study on the sub-fossil microbialites within Laguna del Toro (unpublished publication), southernmost Patagonia, shows how the microbialite multi-scale investigation allied with carbonate carbon and oxygen stable isotopes can provide insights on how microbialites registries the biological (intrinsic) and environmental (extrinsic) conditionings on carbonate precipitation within microbial communities. The deposits are extensive beds of mounds in the lake margins, covered by clusters of m-height pinnacles. Both show thrombolite mesostructure, which is internally composed of a complex assemblage of micritic and microsparitic microfabrics. Domains of interconnected pockets of massive, peloidal, and microlaminated dark micrite are bounded by microsparite. The latter is often crosscut by clotted micrite and structureless mixed micrite and microsparite. The dark micritic domains are formed by subhedral triangular polyhedrons aggregates of Mg-Ca-nanospheres, permeated by mucous-like and honeycomb-like fossilized EPS. The mucous-like features are locally embedding flattened or tubular hollow filamentous cyanobacteria, with 15 to 175 μm long. Microsparite fabrics is composed of limpid, euhedral triangular polyhedrons and rhombohedrons of calcite, with 12 to 20 μm wide. Micrite micro-drilled samples are enriched in 13C (3.02 - 4.69‰ VPDB) and microsparite is lighter (3.36 - 3.81‰ VPDB). Microfabrics and isotopic data suggest that the large micritic domains are formed by early EPS mineralization via photosynthetic CO2 uptake and alkalinity enhancement. Microsparite, otherwise, is interpreted to be associated with degradation of the cyanobacteria-rich biofilms and physiochemical precipitation. Diffuse fabrics (*e.g.*, Clotted micrite) could have been formed by the shrinkage of these cyanobacterial domains, possibly due to heterotrophic or physiochemical processes. The change in microbial-community growth morphology, from mounds to pinnacles, is due to paleolacustrine environmental shifts rather than internal microbial-community modification. It is often difficult to understand the genesis of microbialite structures in the geologic record, because of their lack of biostructures preservation. In this way, this study may serve as an analog to diagnosing and interpreting microbialite structures in ancient carbonate rocks.

keywords: thrombolite; mounds; sedimentology; carbonate precipitation; stable isotopes; paleolacustrine; Magallanes y Antártica Chilena.

1 INTRODUCTION

Microbialites are formed by trapping-binding and various biotic and abiotic precipitation processes associated with microbial communities (Burne and Moore, 1987; Riding, 2011a). The first works characterizing organosedimentary deposits were on stromatolites (laminated structure; *e.g.*, Kalkowsky, 1908; Golubic and Hoffman, 1976). These rocks are the oldest known registries of life, in the Archean (Hoffman *et al.*, 1999), and are registered in up to 85 percent of Earth History (Grotzinger and Knoll, 1999) occurring in diverse paleoenvironments (Riding, 2011b). Although, since the work of Aitken (1967), when thrombolites were defined, plenty of studies on non-laminated microbialites in the geological record have emerged (*e.g.*, Pratt and James, 1982; Walter and Heyes, 1985; Kennard and James, 1986; Guo and Riding, 1992; Kahle, 2001; Harwood and Sumner, 2012; Bosence and Gallois, 2021). The first occurrence of these rocks is abruptly marked in the geologic record at the Neoproterozoic (Awramik, 1971) which proliferate until the Late Cambrian (Kennard and James, 1986; Shapiro and Awramik, 2000), and occur more restricted until the Recent (Shapiro, 2004). These different microbial structures occurring distinctively in the geologic record represent different processes of microbial lithification, thus variations in environmental conditions (Harwood and Sumner, 2012; Suarez-Gonzalez *et al.*, 2019).

The most distinctive features of non-laminated microbialites are the mesoclots (*sensu* Shapiro, 2000) clotted micrite, and peloidal microfabrics, called with different names along the time (Aitken, 1967; Kennard and James, 1986; Shapiro, 2000). Plenty of studies on modern microbialites has proposed the genesis of these features (e.g., Riding *et al.*, 1991; Arp *et al.*, 2003; Dupraz *et al.*, 2004; Dupraz *et al.*, 2009; Burne *et al.*, 2014; Theisen *et al.*, 2015; Bischoff *et al.*, 2020). Although these studies provide essential insights into the mineralization processes involved in lithification, it is often difficult to recognize the exact same features in ancient rocks. Since the modern examples often are not fully lithified and did not undergo significant mineralization, organic matter degradation, and diagenetic alteration.

The alkaline lake Laguna del Toro, in southernmost Chilean Patagonia, contains extensive deposits of sub-fossil lacustrine thrombolites at its margins (not yet described). Extensive beds of domal structures and localized occurrence of meter-high pinnacles are exposed at the margins of the lake. The fully lithified microbialites with

well-preserved structures, along with their distinctive morphology, and the possibility to access elements of paleoenvironmental conditions, provide a unique place to study, on a multiple-scale, the non-laminated microbialite structures.

This paper reports our findings on the genesis of the microbialites within Laguna del Toro. It is, thus, an attempt to provide insights on the intrinsic and extrinsic (*sensu* Dupraz and Visscher, 2005) factors controlling morphology, internal structure, and microfabrics of thrombolites. Accessing these aspects, we can provide information on how biologic processes are registered in the different scales of microbialite features, and how the environment could have controlled it. This information can be valuable to petrologists and sedimentologists studying carbonate deposits in the geological record.

2 GEOLOGICAL SETTING

Laguna del Toro is a small (~15 km²) endorheic alkaline lake in the retroarc of the Austral Andean Cordillera, Magallanes y Antártica Chilena region, Chile (Fig. 1A). It is situated at the lowlands (0 - 200 m) steppe-like plains of the northwestern margin of the Magellan Strait and northeastern margin of Seno Otway. The lake is over the Magellan-Austral foreland basin (Fig. 1B), on top of the glacial-related sediments (Fig. 1C) of the Patagonian Ice-Field fluctuations in the Plio-Pleistocene (McCulloch and Bentley, 1998; Darvil *et al.*, 2015). By the Local Last Glacial Maximum (~35ka; Davies *et al.*, 2020), ice-lobes were spread over eastern Patagonia, occupying the present-day low lands of Magellan Strait, Seno Otway and Skyring (Kilian *et al.*, 2013). With the onset of deglaciation by ~19 ka, the ice retreated forming ice-dammed paleolakes (McCulloch *et al.*, 2005) that, by ~10 ka, were drained into the pacific (Davies, *et al.*, 2020). Since then, Seno Skyring became a part of a fjord system, and land areas with glacial erosive features and related deposits were exposed (Benn and Clapperton, 2000; Kilian *et al.*, 2013). In the Holocene, ice advances were limited to higher altitudes, and climate showed a slight warming trend (Kilian and Lamy, 2012).

Southern Patagonia is on the core of the southern westerly wind belt (~50ºS; Harada *et al.*, 2013). The Andean orogen constitutes a great orographic barrier to the westerlies coming from the pacific. The climate in Patagonia is, thus, a relation between altitude and position relative to the orogen (Carrasco *et al.,* 2002). The Laguna del toro is 50 km east from the orogen lee side, being subject of the dried westerlies, responsible for high potential evaporation rates in eastern southernmost

Patagonia (Garreaud *et al.*, 2013). Therefore, it features a cold transitional sub-humid to semi-arid climate (Coronato, 2008).

Genesis and the evolution of the Laguna del Toro are still unknown. To our knowledge, no bibliography of the lake and neighbors was published. We assume that Laguna del Toro was formed after proglacial lake drainage, during the Holocene, being subject to similar climate conditions to the present and to the southernmost Patagonia during the Holocene.

3 METHODS

Preliminary characterization of hydrology and hydrochemistry of the Laguna was done to correlate modern and possible paleoenvironments. The laguna's geometric and preliminary hydrologic aspects were described at Google Earth Pro. Water sampling and measuring in-situ parameters were done in 2019 September's fieldwork. Lake and river-influx water parameters were measured in-situ by Horiba multiparameter equipment at five locations (Table 1).

Physiochemical analyzes were performed at *Laboratório de Pesquisas Hidrogeológicas* (LPH). Hydrochemistry was characterized by the Piper diagram, at the EasyQuim program. Saturation indexes were calculated at the PHREEQC software (Parkhurst *et al.*, 1982).

The organization and distribution of carbonate and related deposits of the northern-to-eastern lake's margin were recognized at the fieldwork. Morphologic (macrostructure) and mesostructure of the build-ups were characterized. We collected hand specimens of each carbonate structure and powder samples by drilling every 10 cm (vertical) of the best-preserved pinnacles in four localities (labeled TOR II, IV, VI, and VII).

Microfabrics, microstructures, and mineral characterizations were achieved by petrography, Scanning Electron Microscopy (SEM), and X-ray diffraction (XRD) analyses. Twenty-nine thin sections stained with alizarin were analyzed at a transmitted-light microscope. Freshly broken fragments of hand specimens and thin sections were coated by Au-Pd target and analyzed at a JEOL 6010LA coupled with JEOL EX-94410T1L11 Energy Dispersive X-ray Spectroscopy (EDS). Acceleration voltage ranged from 3 to 20 keV and working distance ranged from 9 to 14 mm.

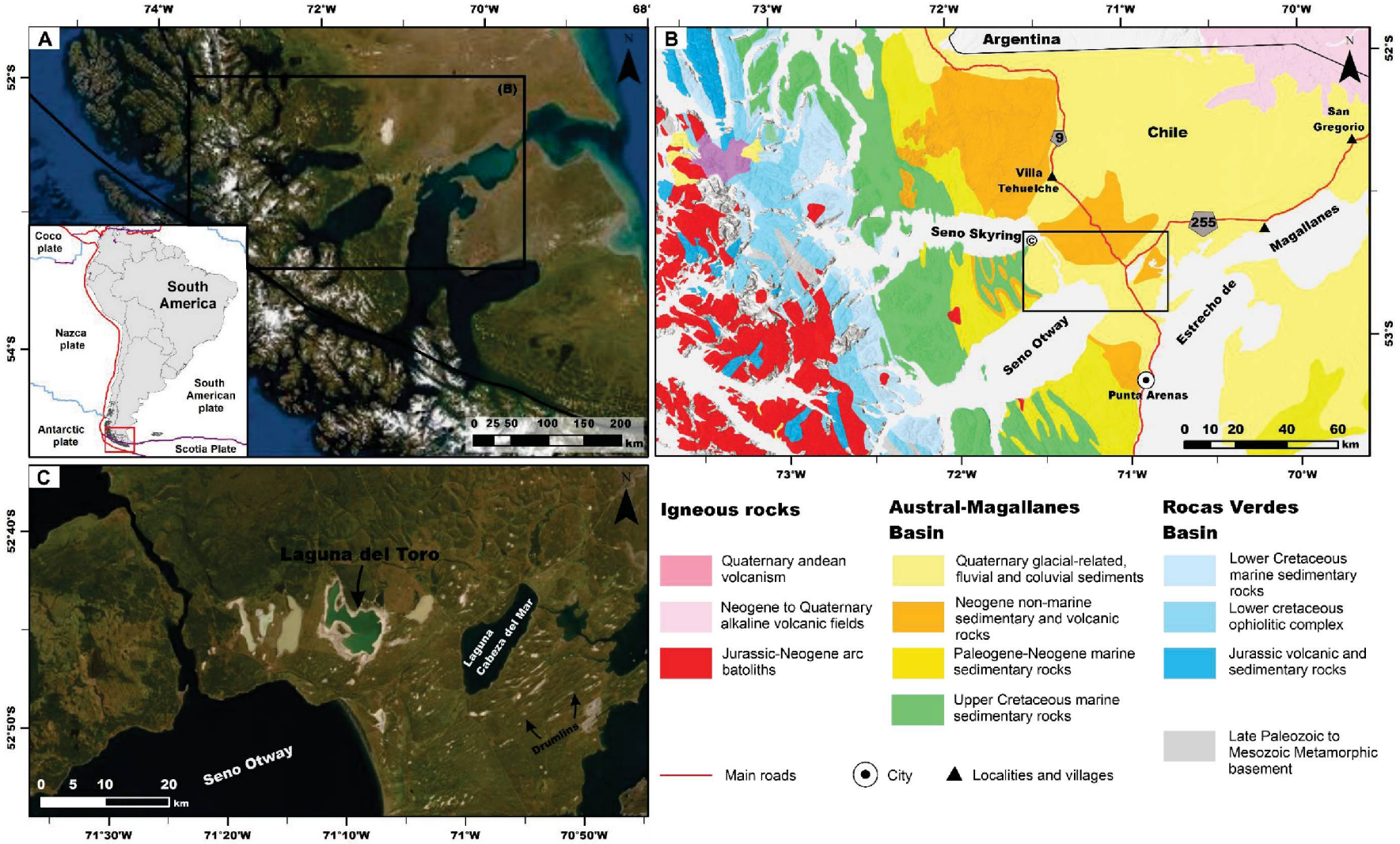

Fig. 1 Laguna del Toro localization. (A) Satellite image of southernmost Patagonia. (B) Regional geological map. (C) Satellite image of Seno Otway northern margin showing Laguna del Toro and surroundings.

Backscattered Electrons (SEM-BSE) images were used to differentiate densities and select the areas for EDS analyzes.

Thirty-one hand specimens were sub-sampled and analyzed by XRD. Bulk-rock mineralogy and semi-quantitative abundance were determined in a Malvern PANalytical Empyrean, with 2θ copper x-ray tubes (Kα λ = 1,54060 Å) configuration. Diffractograms were analyzed in the PANalytical High Score software.

To better understand processes of carbonate precipitation, microbialite, and tufa bulk-rock δ18Ocarbonate and δ13Ccarbonate were determined from 94 drill-collected powder samples. For better resolution on isotope signals, sub-samples of the micritic, clotted, and microsparitic fabrics were collected by micro-drilling of 10 slabs (n=21). Carbonate analyses were performed by the Gas Bench II technique, at a Thermo Fischer Delta V Advantage Isotope-ratio Mass Spectrometer (IRMS). Liberation of CO2 obtained by carbonate digestion using an orthophosphoric acid at 72ºC. Isotopic composition is reported in deviation per mill (δ‰), normalized to the VPDB standard, with 0.1‰ maximum analytical error.

3.1 TERMINOLOGY

We use a multi-scale approach for microbialite describing (as proposed by Shapiro, 2000 and Riding, 2000). We divide the description into megastructure (field description), macrostructure or morphology (outcrop), mesostructure (hand specimen), and microfabrics or microstructures (microscopy or scanning electron microscope; Shapiro, 2000). The latter refers to features formed in microbial-scale, such as crystal type, shape, color, and arrangement. In this way, the term pinnacles and mounds refer to the macro-scale structure and thrombolite refers to the microbialite with mesoclots (*sensu* Shapiro, 2000).

4 RESULTS

4.1 HYDROLOGY

Modern Laguna del Toro is a pale green-colored endorheic lake, with a 13.8 km2 area. The water table is constantly perturbed by the strong westerlies coming from the Seno Otway, resulting in waves zones at the eastern and northeastern lakeshores. Water inflows by surficial runoff and by two perennial channels (Fig 2. A).

Water physiochemical data are summarized in Table 1. It shows pH values ranging from 8.72 to 8.89 and temperature from 4.8ºC to 9ºC during the day (no specific time of sampling). It is an alkaline lake (mean Alk= 37.89 meq/L), Na-Cl type, with moderate DIC concentrations and ionic abundance of $Cl>Na>SO_4>HCO_3$. Saturation indexes of calcite, dolomite, and aragonite are above 1 (10-fold supersaturation), which is the minimum for carbonate precipitation proposed by Arp *et al.* (2001).

Inflow water from the river is overall ionic depleted and hotter than Laguna. Its salinity is 0.593 g/L, pH is 8.83, and alkalinity of 4.81 meq/L. Is relative Ca-enriched, shown by Ca-Mg of 2.8. In the mixing zones of these waters with lake water occur biofilms (see next section).

Table 1 - Lake and river water chemistry and stable isotopes data from Laguna del Toro. Physiochemical data was obtained by several analyzes at LPH.
*Saturation indexes calculated on Phreeqci software.

ID	Location	In-situ	Physiochemical data									Saturation index*		
		pH	T	Salinity	Alk	DIC	Ca	Mg	Na	K	Cl	SO4	Cal	Dol	Ara
			ºC	g/L	meq/L	meq/L	meq/L	meq/L	meq/L	meq/L	meq/L	meq/L	Ω	Ω	Ω
1	lake surface	8.89	8.0	73.7	34.8	34.7	16.0	69.1	853.4	32.8	905.2	208.0	2.2	5.1	2.1
11	lake surface	8.84	5.7	-	-	-	-	-	-	-	-	-	-	-	-
21	river	8.83	9.0	0.6	4.8	4.8	3.4	1.2	9.83	0.3	5.4	2.5	1.0	1.4	0.8
25	lake surface water	8.72	4.8	-	-	-	-	-	-	-	-	-	-	-	-
26	lake surface	8.8	7.8	80.6	50.0	41.1	11.0	87.2	955.3	36.9	1156.2	108.2	1.3	3.4	1.2

4.2 SEDIMENTOLOGY

The flat-sloped northern margins of Laguna del Toro (Fig. 2A) are covered by gravel deposits (mainly cobble- to boulders), lacustrine-related carbonate, and siliciclastic deposits. Gravel deposits are poorly sorted sub-rounded striated sediments, probably, with glacial-related sedimentation. They are exposed at the outer parts of the margins, at about 50 - 300 m from the modern lake. Lacustrine-related deposits (carbonate and siliciclastic) are covering the gravels, therefore occur in the inner part of the margins, closer to the current lake level. They occupy the low altitude (11 - 14 m a.s.l) and low gradient areas, not being found in the steep and higher topographies (cliffs with up to ~35 m a.s.l).

Carbonate deposits are almost continuous outlining the modern lake and cover most parts of the walked area (12 km long, up to 300 m wide) from the modern lake. Preserved or partially eroded fossil- to subfossil microbialite build-ups compose most of these deposits. Their reworked fragments constitute secondary (allochthonous) deposits and are less volume expressive.

Build-ups can be divided into two morphology-types based on the macrostructure of individual heads: pinnacles and mounds. Pinnacles, the most outstanding structures, occur from the northernmost to the easternmost margins (Figs. 2B, 2C, 2D). These are m-height columnar structures, that occur in N/NW aligned clusters of discrete or coalesced big structures (>1.5m; Fig. 2B), non-aligned clusters of packed big structures (Fig. 2C), or as dispersed discrete small structures (<1.5m), which occur in the long E-SE margin (Fig. 2D). Pinnacles were found a few meters from the current lake level (Fig. 2B), tens of meters (Fig. 2C), or hundreds of meters from it (Fig. 2C). These clusters constitute megastructures of agglutinated structures, with few (<10 m^2) to hundreds of square meters (up to 900 m^2) of area.

Figure 2D shows small dispersed pinnacles and, closer to the lake, smaller reddish structures. These are the mounds, cm-to-m-height dome-shaped structures. They are stratigraphically under and beside pinnacles, occur almost continually in all studied margins, as extensive beds (planar megastructures; Fig. 2E) of individual domes that, locally, are submerged (Figs. 2D, 2F). Mounds make up the biggest portion of carbonate deposits, covering a great area (up to 100 m wide and km-long outlining the lake).

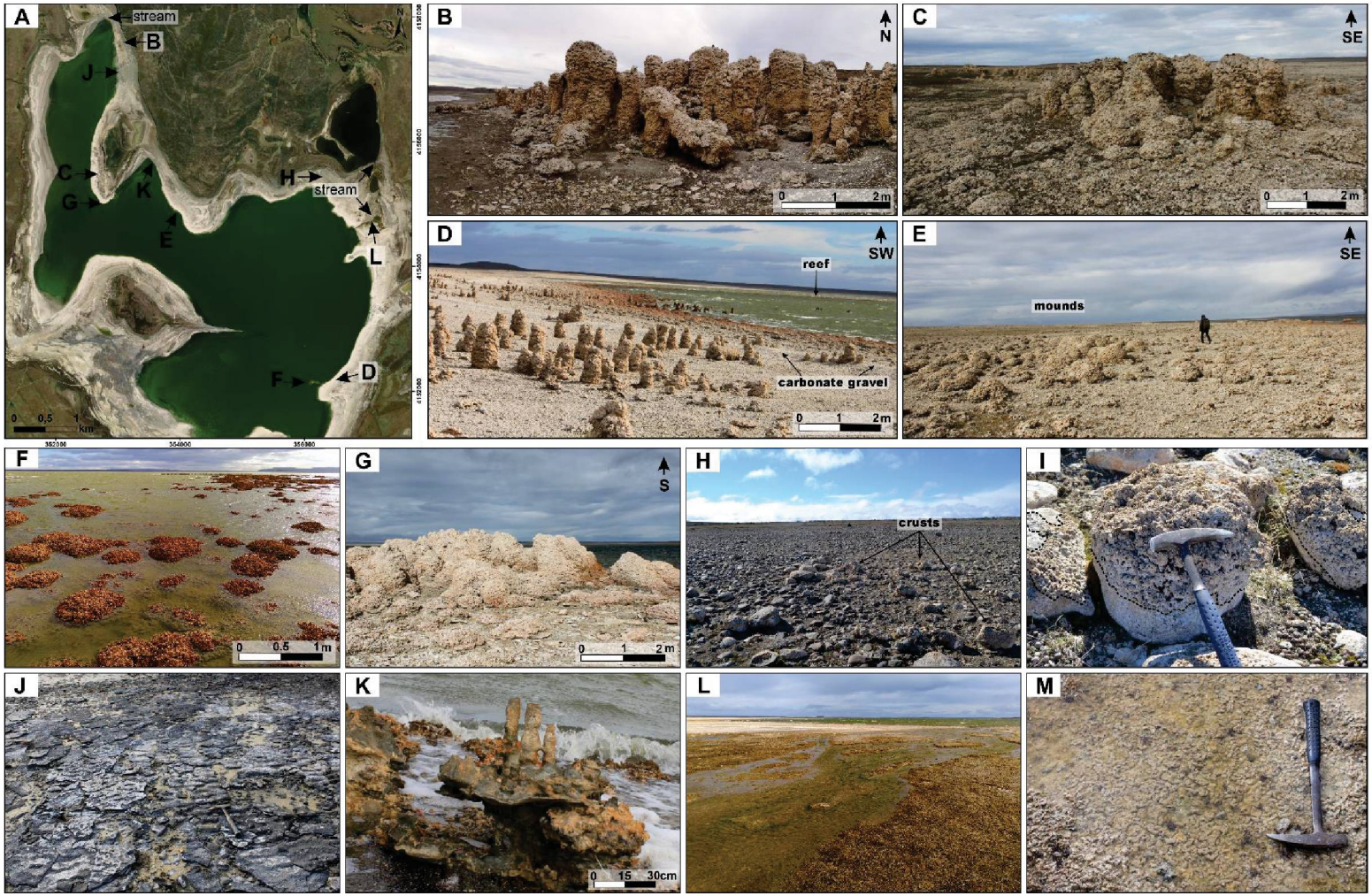

Fig. 2. Laguna del Toro carbonate and carbonate-related deposits. (A) Satellite image of the Laguna with localization of the photos. (B) Northern margin aligned pinnacles. (C) Pinnacle deposit with square morphology, northern peninsula. (D) Dispersed and smaller pinnacles of the E-SE margin. (E) The extensive bed of mounds that covers a great part of the margins. (F) Mound reef at the southeastern margin. (G) Mound cluster at the northern peninsula (bioherm megastructure). (H) Glacial-related boulder deposits ~50 m from the modern lake, with thrombolite crust on the top of them (I). (J) The pavement of beach rock with ripples between mounds. (K) Calcified beach rocks ('sand tufa') with pinnacle morphology. (L) Northeastern green-colored braided stream. (M) Detail of thin wrinkly microbial mat at shallow ponded areas of the stream in 'L'.

can occur in bioherm megastructure (~3 m height and ~15m wide, Fig. 2G). It consists of lateral and vertical irregularly stacked individual mounds.

Carbonate crusts are the farthest (from the lake) primary carbonates, found covering the boulders (Fig. 2H). They consist of cm-thick crusts of pale grey carbonate with clotted mesostructure (Fig. 2I).

Eroded and reworked fragments of microbialites fill interstitial spaces between microbial heads, but also form larger dune-like sheets of non-cemented carbonate gravel (Fig. 2D). Constituted by sub-rounded, non-spheroidal, poorly sorted, porous fragments of microbialites. Forming dm-thick and sinuous elongated crests.

Occurring extensively, detrital deposits are characterized mainly by organic-rich muddy-ooidal sands and mud. They are mainly soft sediments of dark color, that can bury a few centimeters of the build-ups base, or early-cemented rocks. Figure 2J shows, at the base level of the mounds, a pavement of cm-thick beach rock, consisting of muddy-ooidal sand with ripple structure, cemented by carbonate. In Figure 2K, rippled sandstone is covering small mounds, and shows dm-sized (up to ~30 cm) pinnacle morphology, resembling the 'sand tufa' from Jagniecki *et al.* (2021).

Active lithifying mats related to the mound and pinnacles were not found. Although, at the shallow waters of the eastern distributary river (Fig. 2L), microbial mats were found (Fig. 2M). The cm-thick green wrinkled structures have small (mm-sized) carbonate particles, but no evidence of preservation, and so lithification, was found.

4.2.1 Microbialites macro- and mesostructure

Table 2 summarizes the main features of the microbialites. Mounds are the base of carbonate deposits, occurring as extensive beds of locally- to sporadically linked structures (Fig. 3A). They are dome-like thrombolites of pale-grey carbonate, often with a surficial red-colored alteration. They are grown over

Table 2 – Description of mounds and pinnacles within Laguna del Toro

Macrostructure	Mesostructure	Description	Size	Substratum	Occurrence
Pinnacles	Clotted: Interconnected mesoclots (rounded, subrounded and amoeboid), sparse to densely-packed (agglutinated); Clotted laminated: mesoclots with wrinkled lamination; Tufa facies;	Mostly discrete columnar structures of greyish carbonate; Locally lateral coalesced, set of pinnacles can make square forms; Constringed variability of growth; Bigger ones are inclined, sinuous or recumbent; Dichotomous branching is common	Great: Up to ~300 cm height and ~30-70 cm wide Small: Up to 150 cm height and 30-75 cm wide	Coalesced above mounds (when close to lake's margin) or quaternary glacial boulders' deposits	NNW/NNE aligned clusters of the great ones at the northeastern lake's margins; smaller ones are dispersed at the E-SE margins (~50m far from the lake)
Mounds	Clotted: Interconnected mesoclots (rounded, subrounded, and bushy-like), mainly densely-packed (agglutinated);	Closely spaced dome-like (subspherical to nodular) structures of grey to reddish carbonate; Circular to subcircular in plain view; Locally linked lateral coalescence; Interlayering with cm-sized muddy ooidal sands flat layers	From ~10 up to 150 cm height and 20-150 cm wide	Lacustrine muddy ooidal sands and beach rocks; Boulders;	Lake's N to SE margins; Small ones occur as extensive pavements at the margins, sometimes forming reefs inside the lake; Bigger ones (>30 cm) are localized

middle (~20 – 175 cm) and abruptly terminate on a convex-up nodular morphology (Fig. 3B, C).

In plan-view, they are circular to sub-circular. Their size is variable, most structures are up to 40 cm in height, but bigger ones (up to 150 cm high; Fig 3C) occur locally and randomly. At the northern margin, mounds tend to be bigger and have interlaying with cm-thick (~1-5 cm) layers of dark muddy ooidal sand at their bases (Fig. 3C, D).

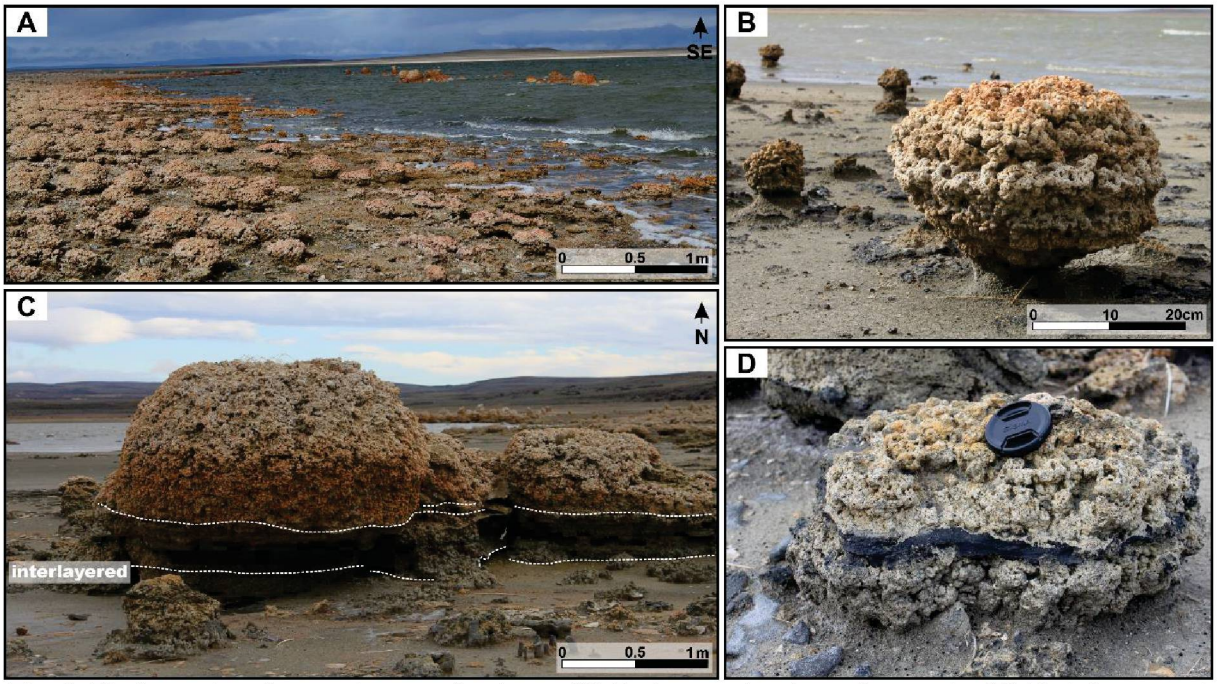

Fig. 3. Photographs of mound macrostructure. (A) Bed megastructure of mounds. (B) Nodular mound rooted on muddy sand. (C) Laterally-coalesced mounds with mud interlaying. (D) Dark cm-sized organic matter-rich muddy sand layer inside the small and eroded mound.

Pinnacles are mostly rooted on the mounds (Figs. 4A, C, D, E) or, farther from the lake, on gravels clasts (Fig. 5B). Structures are slender (~30-75 cm wide) columns with constringed variability of growth (centimetric variance in width; Fig. 4C). They present size, morphology, and distribution differentiation dependent on geographic location. At northern margins, pinnacles are bigger (up to 100-300 cm high, 30-70 cm wide; Fig. 4C, D, E), otherwise, at the E-SE margins, they are smaller (~50-150 cm high, 30-70 cm-wide; Fig. 4F).

The bigger ones are closely spaced clustered, linked to each other by the mounds at their basis (Fig. 4C). Pinnacles can show bridges (Fig. 4D) when closely spaced. In some localities, they are packed in a square morphology feature (Fig. 4D). Giant pinnacles (<300 cm; Fig. 4E) from Laguna del Toro were found in aligned

clusters of up to ten individuals. These show parallel-divergent lateral branching at its upper half and are often epinastic (Fig. 4E).

Figure 4F shows the smaller, more spaced (>100 cm), not branched pinnacles. Besides size and distribution, they show the same slender with variable thickness morphology.

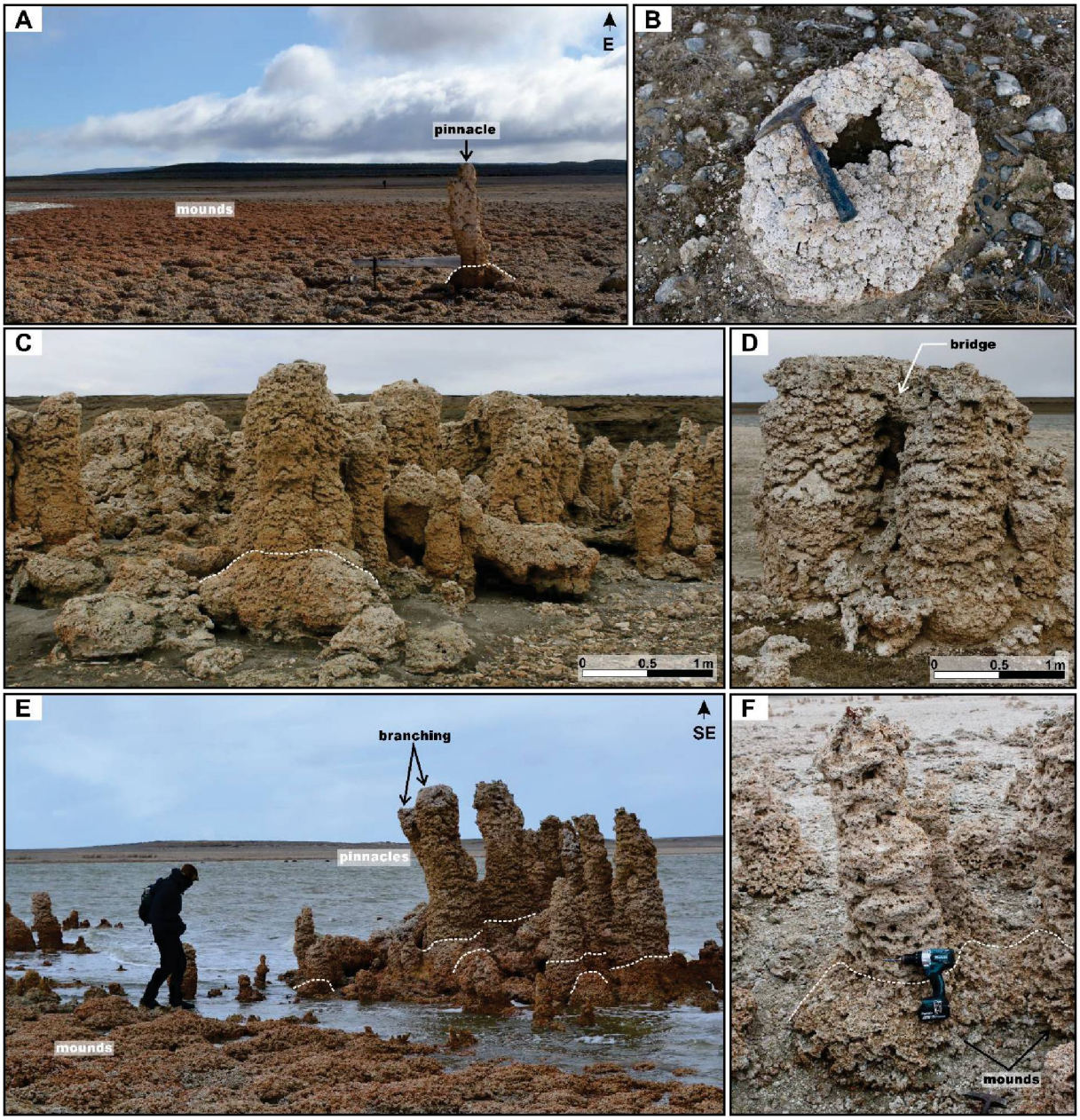

Fig. 4. Photographs of pinnacle macrostructure. (A) Pinnacle over a mound. (B) The hollow base of an eroded pinnacle rooted on gravel. (C) An NNW-aligned cluster of pinnacles. (D) Closely-spaced pinnacles with bridges and square morphology. (E) A cluster of giant pinnacles grown over mounds (dashed line). (F) The smaller and more spaced pinnacles of E/SE margin.

Mounds and pinnacles do not show significant mesostructural differentiation (Fig. 6). Their internal structure seems a continuum, that varies gradually and irregularly along with the build-ups, showing no macrostructural dependence. The

general mesostructure is characterized by agglutinated (mm-sized) rounded to subrounded mesoclots, outlined by a complex irregularly interconnected vugs net. Agglutination gives the overall aspect of the structure. It varies, inside the build-up, in shape, size, and packing density. Millimeter-sized clots are overgrown forming mainly lobate or arborescent-like cm-sized features.

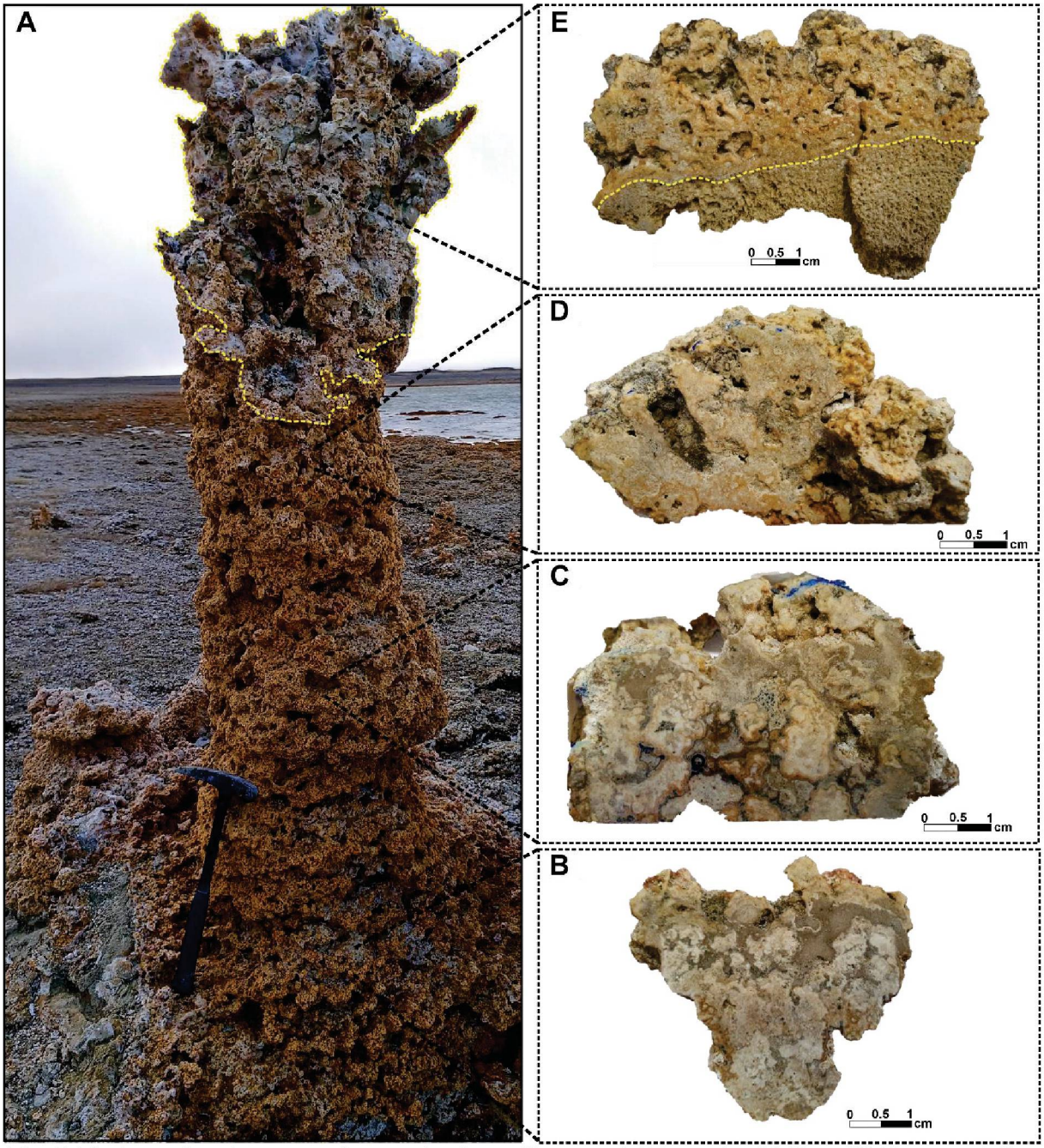

Fig. 5. Photography of macro and mesostructure of Laguna del Toro microbialites. (A) Representative pinnacle over a mound with the virtual position of the samples. (B) Densely packed mesoclotted thrombolite with grey micritic pods. (C) Thrombolite with lobate package clots and circumflex microlamination. (D) Thrombolite with less densely packed and homogeneous mesoclots. (E) Contact of thrombolite and bubble facies, at the top of the pinnacle.

In Figure 5B, mesoclots of the mound are densely-agglutinated and in a slightly arborescent shape. Clots are composed of pale-grey to yellowish-grey carbonate with

irregular mm-sized pockets of grey micrite. These can be lenticular, wrinkled, or horizontal-elongated forms. In Figure 5C the agglutination forms a lobate feature, with an overall similar mesostructure to the mound one. In 5D and 5E, clots are more homogeneous, less densely packed, and without bigger micritic pockets. At the top of the pinnacles (Fig. 5E) is common the occurrence of bubble tufa facies. It occurs irregularly (Figure 5A) but in a well-marked limit with microbialite. It is characterized by friable, elongated carbonate features (mm-sized), surrounded by a complex interconnected porosity.

4.3 MICROFABRICS

Nine microbialite microfabrics (Table 3) were recognized based on grain size, textural relation, and grain arrangement. They are formed by the different arrangements of micrite and microsparite. Therefore, the microbialite framework is mainly constituted by domains of purely micritic fabrics bounded by winding contacts with microsparite.

Figures 6A, 6B, and 6C show the pockets of Massive micrite (MM), they occur in a variety of irregular forms and sizes, with lobate contacts to microsparite. These massive micritic pockets are well-defined domains of pure micrite and detrital grains (<5%). They correspond to the grey micritic pods seen in hand specimens. Often, angular and rounded, non-spheroidal, pyroxene, quartz, plagioclase, volcanic lithoclasts, and intraclasts occur as coated grains dispersed in the micrite matrix. They are covered by thin (1 to 2 μm) laminae of dark micrite.

Inside the pockets, Massive micrite can transit abruptly to Peloidal micrite (PM; Figs. 6A, 6C, and 6F). Peloids can be agglutinated in mm-sized pockets (Fig. 6D) or occur within Clotted micrite (Fig. 6E). Peloids are sub-rounded, non-spheroidal, μm-sized elongated forms. Peloidal pockets are more porous zones than other micritic fabrics (Fig. 6F), they are often half-empty spaces.

Pockets of massive or peloidal micrite are often connected to others by thin micritic laminae (LM; Fig. 6F). Laminae are wrinkled, up to ~100 μm, mostly concentric, that outlines microsparitic domains (Fig. 6G), micritic pockets (Figs. 6H, 6I), and vugs. Rarely, acicular carbonate crystals can be found nucleated inside the micritic laminae (Fig. 6I).

Table 3 – Microfabrics described in Laguna del Toro microbialites

Microfabrics	Description	Mineralogy	Texturally associated with	Occurrence	
				Mesostructure	Macrostructure
Massive micrite (MM)	Rounded pockets (µm-to-cm sized) of dark brown micrite, sometimes with trapped coated detrital grains; Pockets limits are irregular, mainly with lobate contacts, they can be interconnected by irregular micritic patches or laminae; Dense micrite often pass abruptly into peloidal micrite	Low Mg-calcite; Monohydrocalcite (MHC); possibly dolomite	PM; LM; CM; S	Clotted and clotted with grey pockets	Pinnacles and mounds
Peloidal micrite (PM)	Rounded irregular pockets (µm sized) of dark brown, agglutinated, rounded to well-rounded peloids; With 0.5 to 0.7 sphericity; Composed by agglutinated grains of micrite	Low Mg-calcite; MHC	MM; LM; CM; S	Clotted and clotted with grey pockets	Pinnacles and mounds
Micrite laminae (LM)	Wrinkled laminae (10-100 µm wide) of micrite; Often with circumflex morphology outlining micritic pockets, voids, or microspar domains; Contacts with microspar are irregular to lobate	Low Mg-calcite; MHC	MM; PM; CM; S; LM	Clotted and clotted with grey pockets	Pinnacles and mounds
Clotted micrite (CM)	Irregular patches (µm sized) of dark brown micrite surrounded by microsparite or micrite-microsparite matrix (MMS); Contacts with surrounding are irregular to lobate, sometimes poorly defined	Low Mg-calcite; MHC and aragonite	MM; PM; LM; S; MMS; O	Clotted	Pinnacles and mounds

Table 4 – Microfabrics described in Laguna del Toro microbialites (continued)

Microfabrics	Description	Mineralogy	Texturally associated with	Occurrence	
				Mesostructure	Macrostructure
Microspar (S)	Mostly composed of continuous or restricted areas of whitish-grey microsparite;	Low Mg-calcite	MM; PM; LM; CM; O	Clotted and clotted with grey pockets	Pinnacles and mounds
Mixed micrite-microsparite (MMS)	Matrix of unorganized micrite and microsparite; Occur surrounding other micritic fabrics;	Low Mg-calcite; MHC and aragonite	CM; O	Clotted	Pinnacles, mainly at the mid-ranges
Ooidal (O)	Ooids (120 – 400 µm) in three types: rooted in the matrix, with internal lamination connected to the surrounding; with poorly defined internal lamination and limits; well-rounded ooids with well-defined limits and lamination	Low Mg-calcite; MHC and aragonite	CM; MMS	Clotted	Pinnacles
Geopetal (G)	Detrital grains of pyroxene, plagioclase, and quartz in a carbonate, Si and Mg-bearing carbonate mud matrix; Ooids and thrombolite intraclasts can be found	Clinopyroxene, plagioclase, quartz, clay minerals, and carbonates.	None	Clotted and clotted laminated	Pinnacles and mounds; mainly lower parts

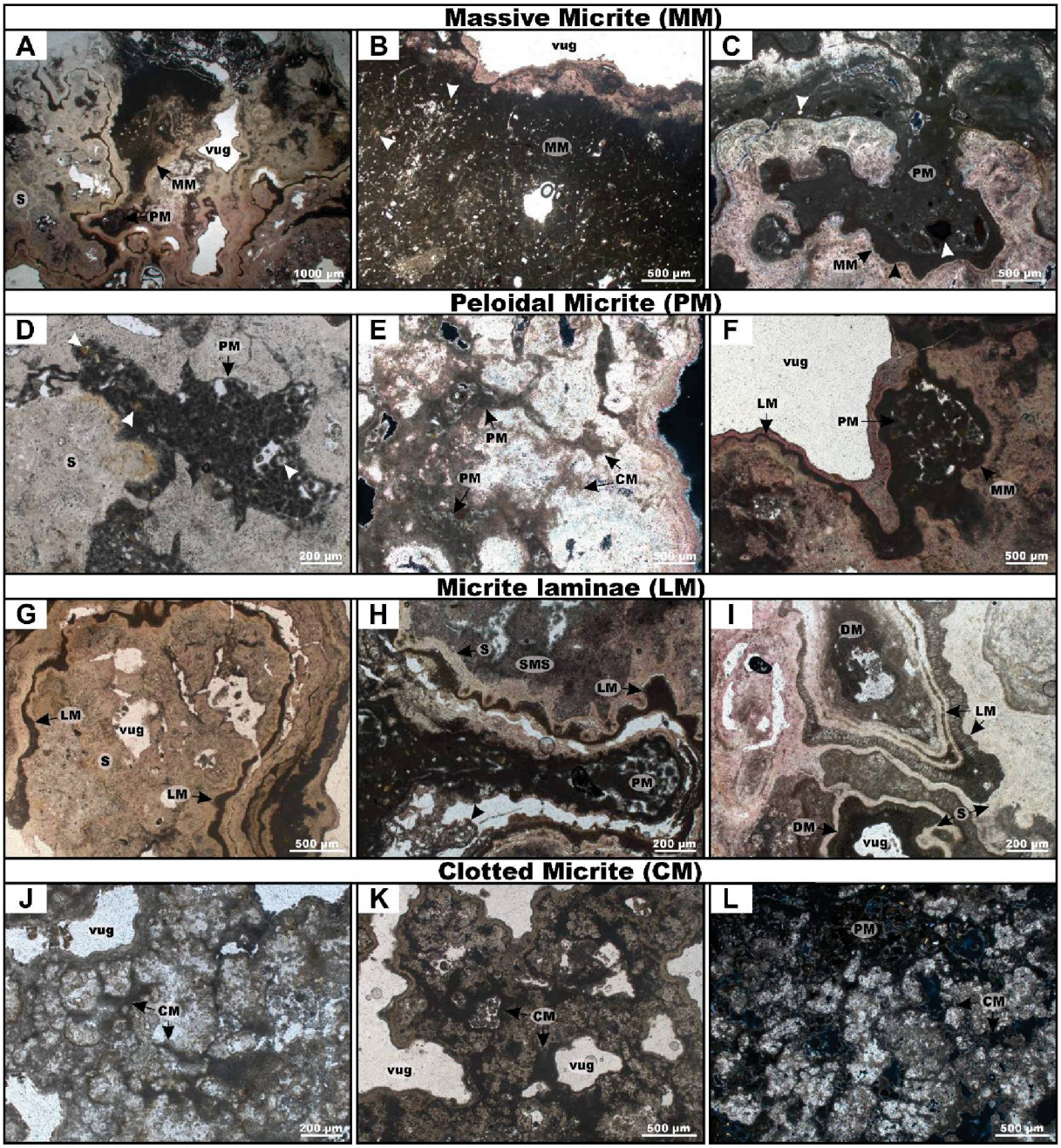

Fig. 6. Thin-section photomicrographs showing microfabrics. (A) A pocket of Massive micrite with an internal pocket of Peloidal micrite. (B) A giant pocket of MM, with detrital grains (white arrows). (C) A mushroom-shaped pocket of massive (outer) passing to peloidal micrite (inner), with lithoclasts and grains (white arrows). (D) A pocket of Peloidal micrite bounded by microsparite. (E) Peloids inside clots. (F) A pocket of massive and peloidal micrite connected to other by laminae. (G) Circumflex microlamination. (H) Micritic laminae outlining micritic pocket with dissolution features (black arrow). (I) Micritic lamination with acicular crystals, outlining micritic pocket. (J) Clotted micrite. (K) Dense patches of micrite. (L) Clotted micrite with peloidal nuclei.

In textural contact with the other micritic domains, or isolated, Clotted micrite (CM; Figs. 6J, 6K, 6L) occur extensively. It is characterized by irregular patches of micrite surrounded by microsparite (Figs. 6J, 6K). When the Clotted micrite forms larger domains (<1000 µm) peloidal micrite can occur at the inner parts of the patches

(Fig. 6L). Sinuous contacts between micrite and microsparite suggest different viscosities in the precipitation medium.

Microsparite microfabrics (S) are homogeneous domains, characterized by whitish-grey zones, of equal-sized subhedral carbonate crystals, around micritic domains (Figs. 7A, 7B). Sometimes micrite and microsparite occur mixed, in a matrix with no structuring (MMS; Fig. 7C). Mixed micrite-microsparite is characterized by carbonate crystals of various sizes with no textural selection. It is often seen where the micrite patches limits are scattered and turn to a more unorganized frame.

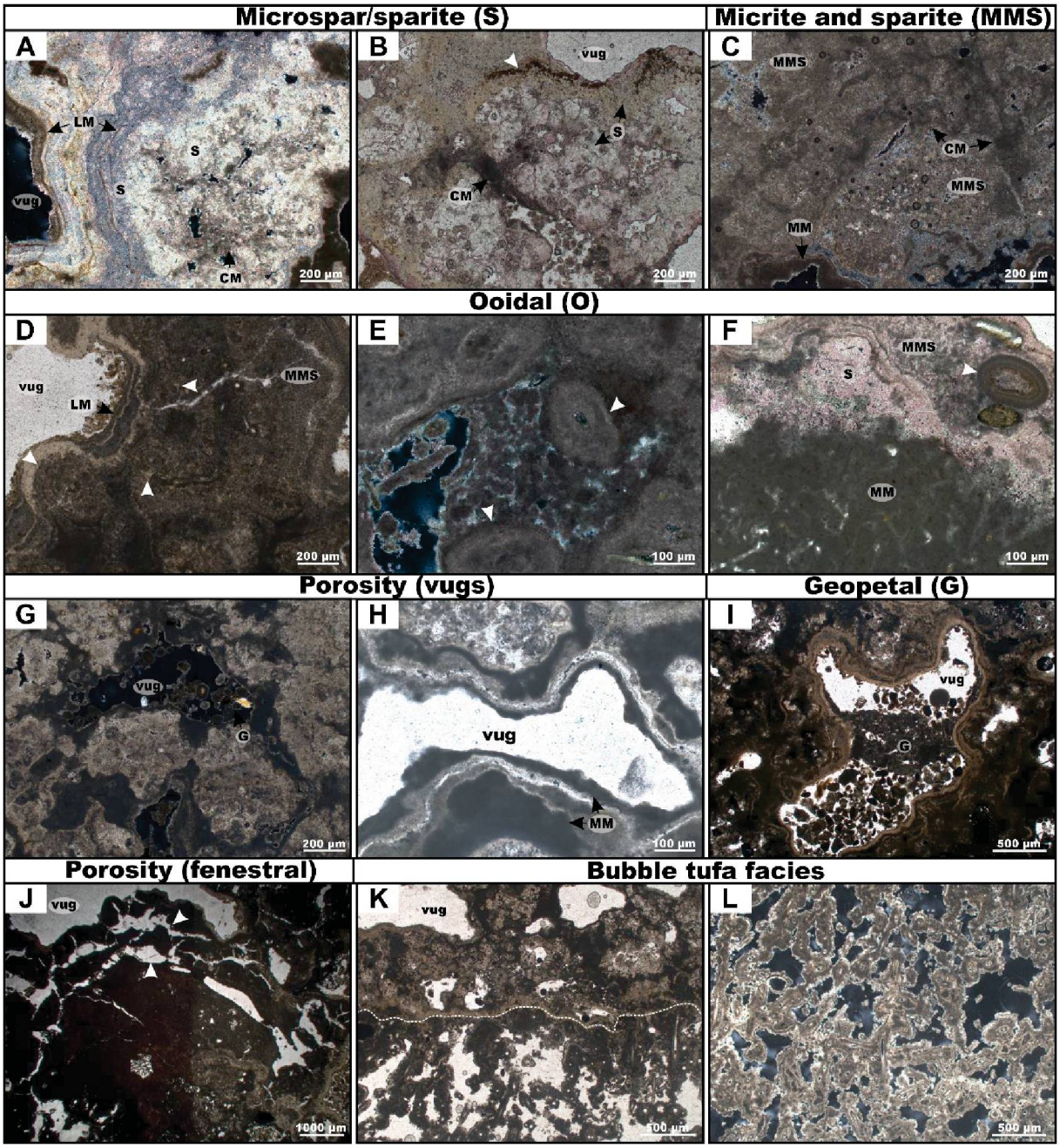

Fig. 7. Thin-section photomicrographs showing microfabrics (continued). (A) Microsparite bounding micritic lamination. (B) Coarser crystals of microspar surrounding patchy micrite. (C) Mixed micrite and microsparite matrix in between clots of micrite. (D) Rooted ooids (white arrows) with detrital nuclei and

internal lamination connected to the matrix (MMS). (E) Irregular ooids inside pocket of peloids. (F) Rounded, well-defined ooid (white arrow) bounded by mixed micrite and microsparite. (G) Vug with few geopetal sediments (G). (H) Vug with a micritic wall. (I) Geopetal filling, composed of sand-sized grains and micritic mud. (J) Fenestral porosity associated with dark micrite. (K) Contact between clotted micrite and bubble facies. (L) Bubble facies, with its micritic spoon-like and elongated features.

Ooids occur in three different types: inside the matrix, with no clear limits, characterized by a grain nucleus, surrounded by concentric micritic lamination continuous to the external micritic matrix (Fig. 7D); as more limit-defined irregular ooids, with a grain nucleus and poorly defined lamination (Fig. 7E); as well-rounded ooids, with clearly defined limits and internal lamination (micrite and microspar intercalation; Fig. 7F).

Primary porosity, in thin section, is mainly characterized by irregular vugs, often contoured by dark micrite (Fig. 7G) and partially filled by sediments (Figs. 7H, 7I). Sediments filling vugs are sand of various compositions and carbonate mud (Fig. I). Fenestrae porosity can occur, not often, and in association with micrite laminae (Fig. 7J).

Bubble facies are in abrupt contact with clotted micrite fabrics. Abruptly, the micrite patches become more organized, forming pellets of micrite rimming an empty nucleus (Figs. 7K, 7L). These changes are marked by an irregular line of dark micrite, which delineates the beginning of the bubble facies.

4.3.1 Microstructure and composition

Examination of the thin sections reveals that the micritic pods, peloidal pockets, and clots are interconnected by micritic laminae (Figs. 8A, 8B). When analyzed at SEM-BSE (Fig. 8C) the micrite microfabrics are compositionally homogeneous and texturally linked. SEM-EDS data indicate that the micrite in the microbialite is Mg-bearing carbonate, in contrast to the microspar, which is purely Ca-carbonate (Fig. 8D).

Scanning electron microscopy photomicrographs of the micrite show anhedral triangular polyhedrons aggregates of Mg-Ca-carbonate nanospheres (<1 μm; Figs. 9A, 9B). Massive micrite and micrite laminae are continuous zones of densely packed aggregates. Peloids are spheroidal (up to 20 μm), mainly ellipsoidal (50 – 375 μm), agglutinations of tightly packed polyhedrons (Figs. 9C, 11C). They are limited by porous and sustained by leaning on each other and on the walls of the pockets. On the surface of peloids, alveolar-arranged flaky crystals are observed.

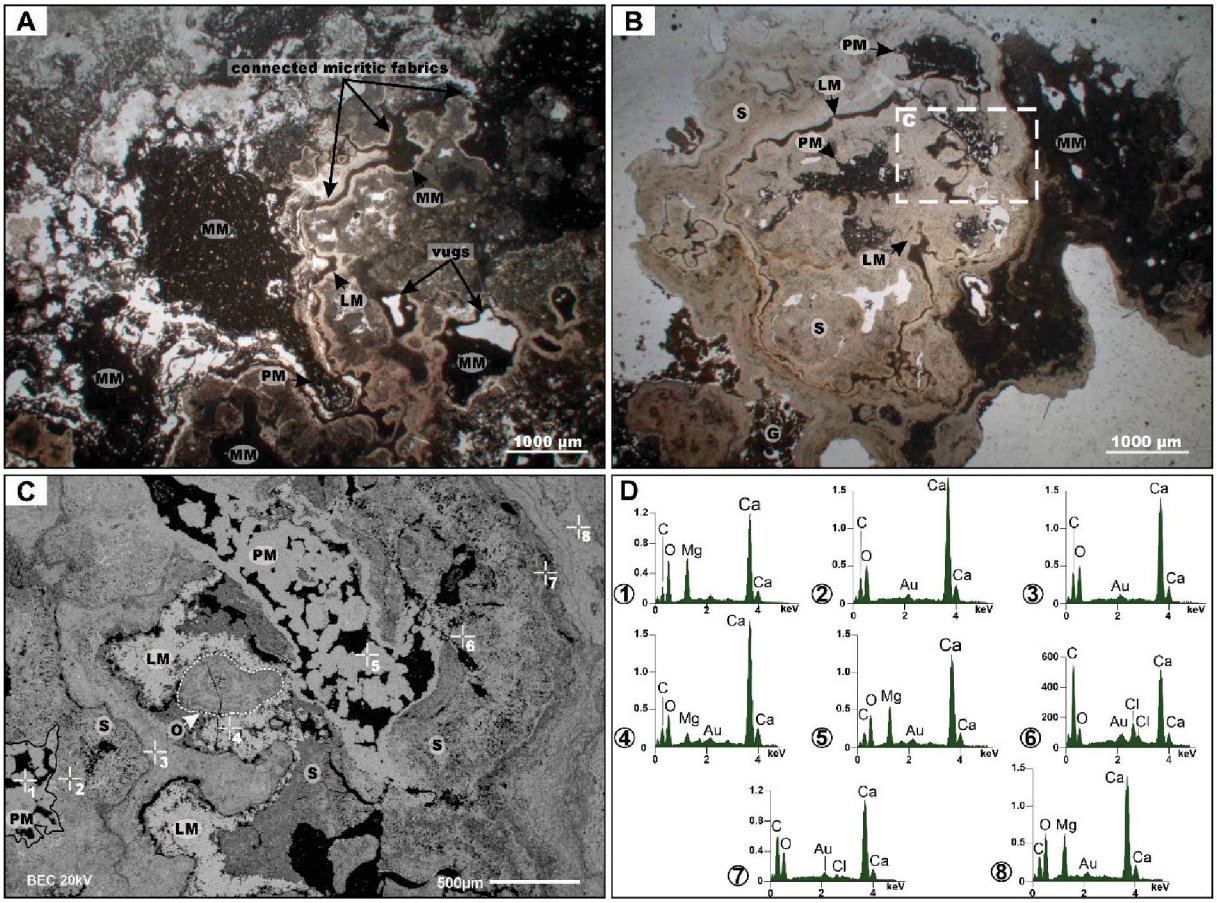

Fig. 8. Microstructures, textural relation, and elemental composition of micritic and sparitic domains. (A) Thin-section photomicrograph showing the micritic microfabrics connected by thin wrinkled laminae (LM) or passing one to another (*e.g.*, MM to PM), note the dissolution features (pink arrow) of the micrite. (B) Thin-section photomicrograph showing connected micritic fabrics surrounded by microsparite. The contact between micrite and microsparite domains is lobate. (C) SEM-BSE image showing insertion of B, each microfabrics and points of SEM-EDS analyzes. (D) SEM-EDS spectral peaks for each point in C. See also supplementary 1.

The most distinctive microspar phase is euhedral polyhedrons (12 – 20 µm) of Ca-carbonates (Fig. 9E). These polyhedrons are characterized by triangular faces (perpendicular to the c-axis) with well-defined vertices, edges, and faces. They are formed by nano-triangular tighten plates (Fig. 9F). Together with the triangular polyhedrons, rhombohedrons compose the microspar and micritic fabrics. Large subhedral (10 - 25 µm) or smaller anhedral (<1 - 5 µm) rhombohedrons, occurs forming the microsparite fabrics (Fig. 9F) and micritic fabrics.

Bulk-rock XRD analyses of 4 samples of a giant pinnacle grown over a mound (Fig. 10) suggest that the main carbonate phases are monohydrocalcite, aragonite, low-Mg calcite, and, locally, dolomite. Semi-quantitative data indicate that monohydrocalcite is the dominant mineralogy at microbialites, the samples in the image contain 40% - 88% MHC, 12 - 41% aragonite, in contrast to 0% - 28% low-Mg calcite and 0% - 16% dolomite. D-spacing data shows that chemical composition within

individual phases is similar in all samples. These results are consistent with the other 16 samples analyzed (see supplementary 3).

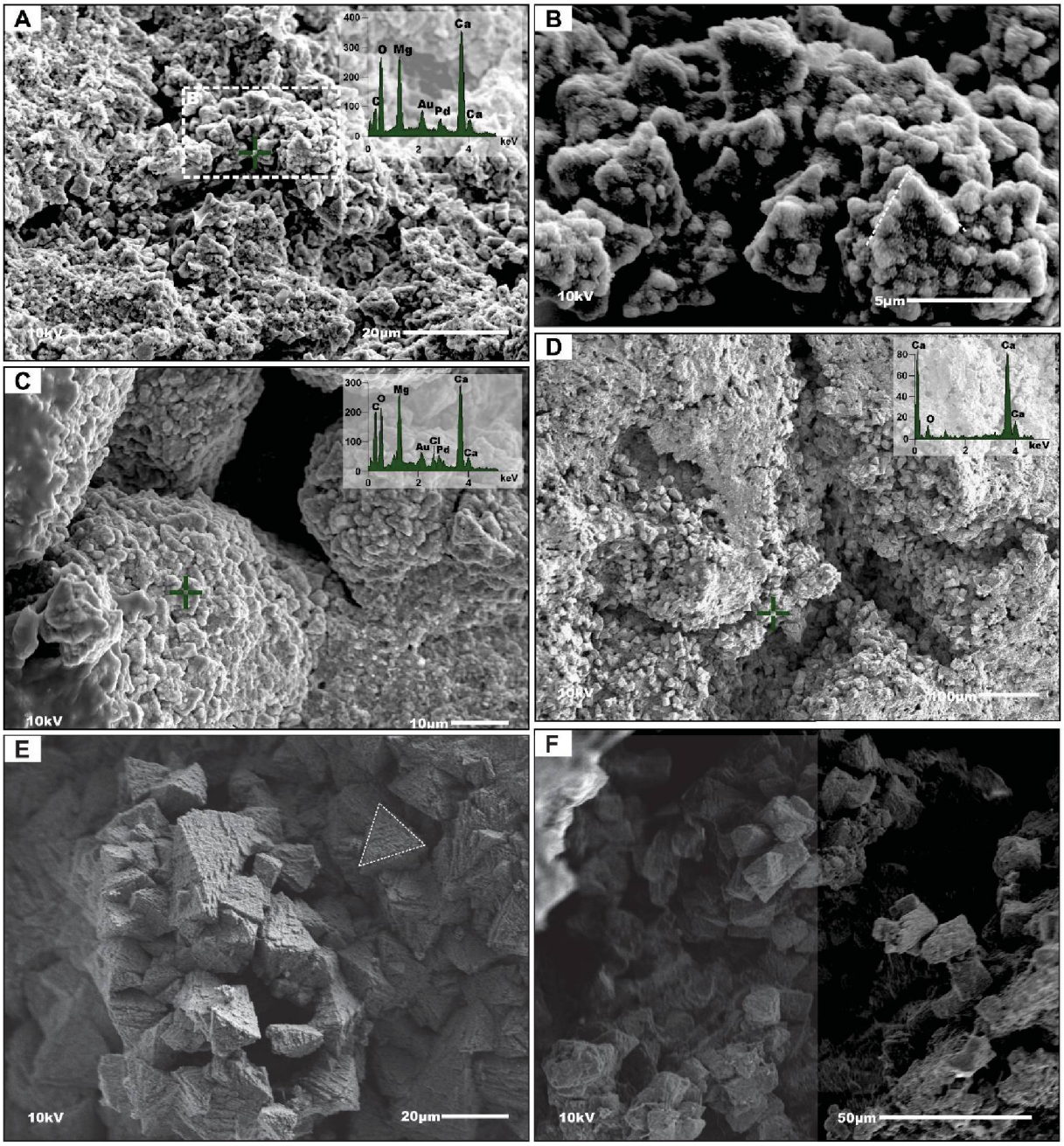

Fig. 9. Scanning electron microscopy photomicrograph of carbonate microstructures. (A) Anhedral triangular polyhedrons aggregates of Mg-Ca-carbonates nanospheres, with EDS spectral peaks. (B) Insertion of 'A' showing nanospheres agglutinated. (C) Mg-bearing carbonate forming peloids, with EDS spectral peaks. (D) Microsparitic domain showing well-formed polyhedrons and EDS spectral peaks. (E) Detail of microsparitic euhedral triangular polyhedrons. (F) Subhedral rhombohedrons of microsparite microfabrics.

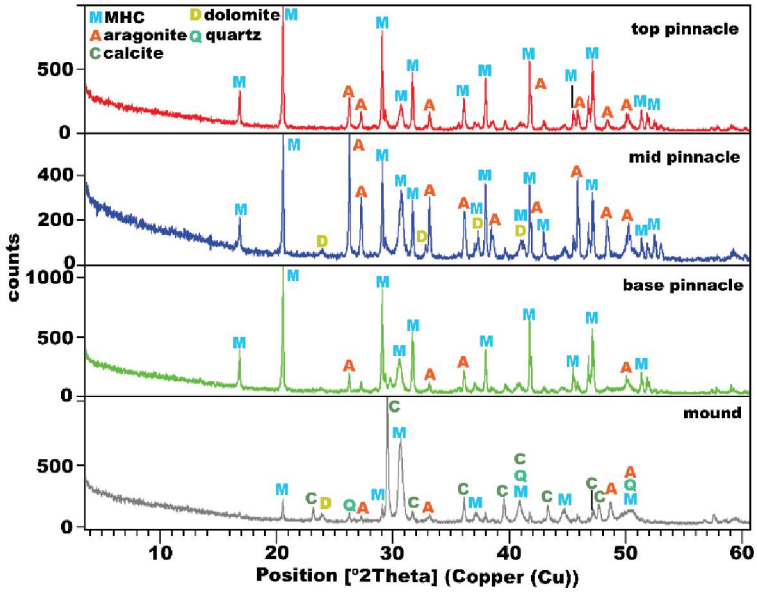

Fig. 10. Selected bulk-rock XRD patterns showing mineralogy of pinnacle grown over a mound. Greyline is the mound's diffractogram, green, blue, and red show the base, middle, and top, respectively, of a giant pinnacle (~2,80m). Monohydrocalcite (4.324-4.328 Å) and aragonite (3.96-3.95 Å) are the most dominant phases. Low-Mg calcite (3.02-3.36 Å) is the third most common mineralogy. Dolomite (2.841-2.915 Å) occurs in a few samples in low percentages.

The dark brown color of micrite in transmitted-light microscopy suggests the presence of organic matter within micritic grains (see also supplementary 2). Scanning electron microscope images show that the Mg-Ca-carbonates are spatially related to fossilized extracellular polymeric substances (EPS). Honeycomb-like networks permeate nanospheres and their aggregates (Figs. 10A, 10B). Film-like features envelop portions of the peloids and make webs between them (Fig. 10C). The low counting of the Ca spectral peaks, and the presence of Si, suggest that these materials have low crystallinity and the presence of diffuse organic matter (Fig. 10C). Smaller (~1 µm) similar features occur around the nanosphere aggregates. These features pass to sheet-like features forming irregular networks, that often wrap filaments of possibly fossilized cyanobacteria (Fig. 10D). Larger and seemingly less malleable folded sheet-like features can sheath a great volume of Mg-Ca-carbonate aggregates, forming hemispherical structures of up to 50 µm wide (Fig. 11E).

Great tubular (up to 175 µm; Fig. 10F) and flat (15 – 45 µm; Fig. 10G) molds of filaments crosscut the Mg-Ca-carbonate aggregates, and are associated with remains of mucous-like features or embedded by them. It is, then, possible to distinguish two distinct morphologies of the cyanobacteria, the great tubular and the flattened. Both of them are mineralized by sub-micron carbonate, possibly with remaining organic matter. On the surface of the filaments, it is recognizable sprouted Mg-Ca-carbonate nanospheres with granular texture (Figs. 10F, 10H).

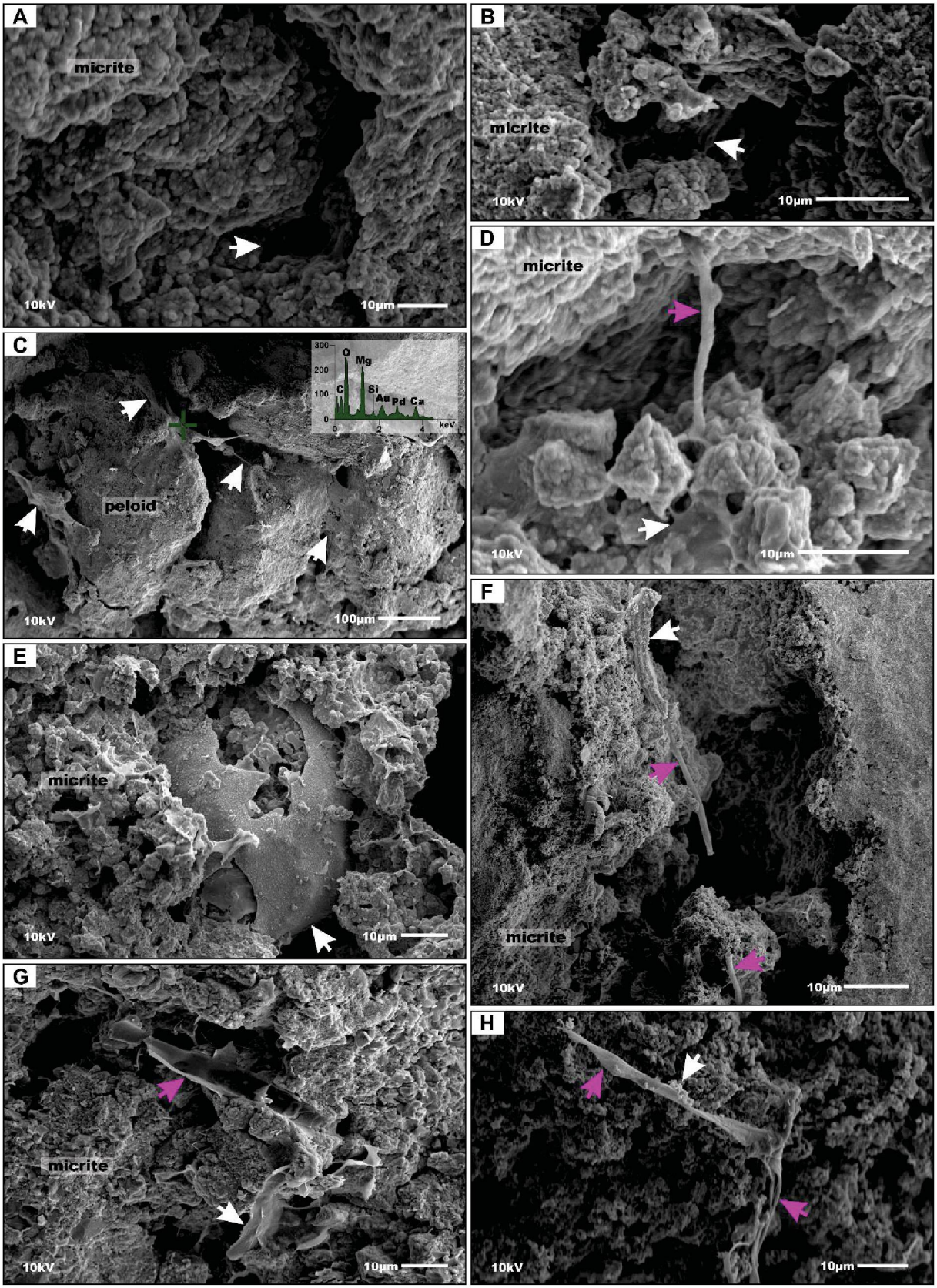

Fig. 11. Fossilized biofilms and filamentous cyanobacteria. (A) Micritic polyhedrons with honeycomb-like fossilized EPS. (B) Micrite permeated by honeycomb-like EPS. (C) Peloids with film-like web features with EDS spectral peaks. (D) Network of film-like and sheet-like features embedding filament. (E) Planar organic feature embaying a pack of micritic crystals. (F) Hollow tubular filaments (pink arrows) crosscutting micrite, over the surfaces of filaments nanospheres are sprouted (white arrow).

4.4 CARBON AND OXYGEN ISOTOPES

In the cross plot of Figure 12, the samples are discriminated into bulk-rock and micro-drilled fabrics. Micro-drilled $\delta^{18}O$ values are slightly more positive than bulk-rock and the variation among microfabrics is comprised mainly in the X-axis ($\delta^{18}O$), but with slight Y-axis ($\delta^{13}C$) variation from the microspar to micrite extremes.

Microbialites signals are with positive covariance (r^2=0.69). They are more overall positive than tufa bubble facies. Pinnacles and mounds do not show any discrimination. Microbialites bulk-rock $\delta^{13}C$ vary between 2.4 - 4.48‰ VPDB and $\delta^{18}O$, between -2.7 and -0.3‰ VPDB (see also supplementary 4). On the other hand, Bubble facies $\delta^{18}O$ data are comprised between -2.51 and -1.73‰ VPDB and $\delta^{13}C$ are between 1.55 and 2.16‰ VPDB.

Oxygen values of the micritic fabrics are comprised between 0.33 and 2.32‰ VPDB, carbon isotope ratios, between 3.02 and 4.69‰ VPDB. Sparitic fabrics present slightly more negative oxygen signals, varying between -1.21 and 0.6‰ VPDB, and $\delta^{13}C$ are between 3.36 and 3.81‰ VPDB. Clotted signals are approximately halfway between extremes of purely micrite and microspar. Their oxygen values are among 0.03 and 0.36‰ VPDB, and carbon values are between 4.02 and 4.14‰ VPDB.

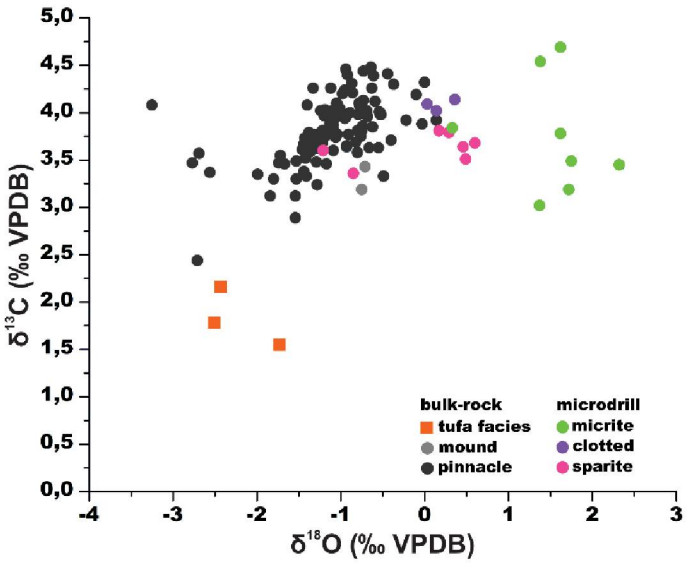

Fig. 12. Oxygen and carbon isotope-ratios of Laguna del Toro microbialites. Bulk-rock and micro-drilled samples are discriminated. Bulk-rock data are of microbialites (mounds and pinnacles) and tufa facies, which refers to the bubble facies. 'Micrite' refers to larger micritic domains (includes MM and PM), 'sparitic' is microsparitic fabrics (S), and 'clotted' is CM.

5 DISCUSSION

Laguna del Toro is a modern alkaline and saline endorheic lake. At the northern, northeastern, and eastern flat margins of the lake, we found glacial-related deposits partially covered by unique sub-fossil microbialite structures. The microbialites show an internal thrombolitic framework, texturally composed of the relation between micritic and microsparitic domains.

5.1 MINERALOGY

It is often difficult to recognize the exact mineral phase in fine-grained carbonate rocks composed of various carbonate minerals, being necessary the intersection of XRD and SEM data. Our preliminary bulk-rock X-ray diffractometry results suggest that the main mineralogic phases are monohydrocalcite, aragonite, and low-Mg calcite. Several studies have emphasized that monohydrocalcite incorporated different amounts of Mg in its structure, and its stabilization is preferable in low temperature (3 - 5ºC), high pH (>9), high alkalinity, magnesian, phosphate-rich aqueous medium (Li *et al.*, 2008; Rodriguez-Blanco, 2014; Lin *et al.*, 2018; Pan *et al.*, 2019; Kitajima *et al.*, 2020; Vereshchagin *et al.*, 2021). Monohydrocalcite formation requires high supersaturation states, which, in natural environments, are most likely reached by the metabolic creation of supersaturated microenvironments (Párraga *et al.*, 1998). Despite being metastable in relation to calcite or aragonite, there is a registry of 800 ka preserved MHC (Solotchina *et al.*, 2009).

Thus, we interpret that MHC is the main constituent of micrite, as these domains are magnesium-rich and associated with biostructures. Monohydrocalcite could be primary or ikaite reprecipitation (*e.g.*, Dahl and Buchardt, 2006). The latter is a low-temperature calcium carbonate polymorph (Bischoff *et al.*, 1993), with reported occurrence in Patagonian lakes during the Holocene (Oehlerich *et al.*, 2013). Due to XRD data and morphology of the micrite crystals, Low-Mg calcite probably occurs with MHC. Although, conditions necessary for MHC formation may inhibit low-Mg calcite precipitation (Mucci *et al.* 1989; Nielsen *et al.* 2016). This leads us to the possibility of calcite and, in less quantity, dolomite, being secondary minerals, formed by the destabilization of MHC (as in Rodriguez-Blanco *et al.*, 2013). In this way, their quantity could be an inverse product of MHC preservation, which depends on time, water-phosphate availability, and pH (>8; Lin *et al.*, 2018). We do not rule out the possibility

of dolomite primary precipitation, once it can be formed in Mg-rich solutions at low temperatures (Vasconcelos *et al.*, 1995).

The XRD results show different d-spacing values, thus, different Mg-content within calcite (supplementary 3). Whilst the values are in the Low-Mg calcite spectra (Zhang *et al.*, 2010), they indicate calcites with different magnesium contents. The microsparitic triangular and rhombohedral polyhedrons are distinctly calcite, and their EDS peaks do not indicate magnesium content. Thus, primary calcites with no Mg content may compose microsparite, and those with higher Mg content are the secondary minerals within micrite. Acicular distinctive crystals of aragonite were only seen in micritic domains at light-transmitted microscopy, but, by the chemical conditions, we suggest that most of the aragonite occurs with calcite in microsparite.

Further investigation is needed to better characterize the mineralogy of the Laguna del Toro microbialites. Mainly, the occurrence, formation, and preservation of monohydrocalcite, which are not well documented in microbialites.

5.2 MICROFABRICS AND MINERALIZATION

Plenty of evidence suggests that micrite and microsparite fabrics were formed by distinct precipitation processes. Micritic fabrics present a range of biostructures absent within microsparite. Their dark brown crystals, under SEM, show Mg-Ca-carbonate nanospheres aggregated, permeated by three-dimensional honeycomb-like, film-like, and planar mucous features. These, consistently resemble honeycomb structures of non-degraded EPS in living microbial mats (*e.g.*, Defarge *et al.*, 1996) and the partially degraded EPS in mineralized mats (*e.g.*, Spadafora *et al.*, 2010; Perri *et al.*, 2012; Bischoff *et al.*, 2020).

The fossilized EPS is often embedding filamentous, presumably, cyanobacteria microfossils. They occur as isolated bodies or in small clusters, with flat or tubular hollow morphologies, sometimes forming molds in the micritic matrix. Some studies have suggested that mechanisms of fossilization via ion adsorption by the surface of the cells (*e.g.*, Sergeev *et al.*, 2002; Van Lith *et al.*, 2003), and others, entombment of the cell regarding carbonate precipitation induced by metabolic bacteria activity (*e.g.*, Arp *et al.*, 2001; Couradeau *et al.*, 2013).

The molds of the filaments are approximately the same width as the body itself, indicating that they did not undergo significant desiccation before fossilization (early mineralization). This, along with the consistent relationship between EPS formation

and micritic nanospheres, suggest that cyanobacteria played an important role in Mg-Ca-carbonate precipitation.

Papers on modern microbial mats in saline systems have shown that mineralization of cyanobacteria EPS may be by: (I) Photoautotroph alkalinity enhance (Burne and Moore, 1987; Merz, 1992; Arp *et al.*, 2001; Ludwig *et al.*, 2005) (II) *sensu strictu* organomineralization (Defarge and Trichet, 1996; in Dupraz *et al.*, 2009); (III) EPS degradation by heterotrophic bacteria (Arp *et al.*, 1999a, b; Dupraz *et al*, 2004; Dupraz and Visscher, 2005; Riding and Tomás, 2006); (IV) extrinsic saturation of the EPS binding capacity. Studies on alkaline lake microbialites have suggested that the EPS, due to pH buffering of the high DIC waters, rather inhibit calcification than induce it, and precipitation would occur by heterotrophic consumption of it (Arp *et al.*, 1999a, b; Arp *et al.*, 2001; Arp *et al.*, 2003; Dupraz *et al.*, 2009). This would progressively release the bound ions into the alkaline environment leading to the precipitation of nanoglobules that coalesced into polyhedral crystals (Sprachta *et al.*, 2001; Dupraz *et al.*, 2004). Continued mineralization could lead to peloid formation (Spadafora *et al.*, 2010) that would be followed by physiochemical precipitation in the opened spaces (Dupraz *et al.*, 2004; Dupraz and Visscher, 2005).

The resulting features of the heterotrophic-induced precipitation closely resemble the Clotted micrite and Mixed micrite-microsparite fabrics. Although it may not be the mineralization process of the large pockets of massive and peloidal micrite. The extensive pockets with continuous micrite and lobate contacts with the bounding microspar do not fit with these features. It is possible that the early mineralization of the EPS occurred by the alkalinity gradients within the microbial mats, as a result of the photosynthetic uptake of CO_2 and H_2CO_3 increase (Merz, 1992; Merz-Preiß and Riding, 1999; Merz-Preiß, 2000; Arp *et al.*, 2001; Ludwig *et al.*, 2005; Aloisi, 2008; Couradeau *et al.*, 2013). To overcome the problems stated by Arp *et al.* (1999a) and Arp *et al.* (2001), it possibly would be necessary an external fluid discharge, to increase the Ca^{2+}, Mg^{2+}, and decrease DIC concentrations (Arp *et al.*, 1999b; Chagas *et al.*, 2016). Although, experimental studies (*e.g.*, Ludwig *et al.*, 2005; Shiraishi, 2012) have shown that photosynthetic-led precipitation could occur despite the high DIC concentrations of alkaline hypersaline lakes.

Following the proposed process of Massive micrite formation, the peloids thus may have been formed in association with that microfabrics. The SEM images of peloids within pockets inside Massive micrite show that the Mg-Ca-carbonates

polyhedrons of Massive micrite are the same agglutinated forming the peloids (Figs. 9C, 10E). Moreover, both show the same mucous biostructures. Kazmierczak *et al.* (1996) suggested that homogeneous micrite and micritic peloids were distinct fabrics formed in a continuum of the same process. Dense micrite was mineralization of photosynthesizing coccoid cells, some groups of cells would not be calcified and with the post-mortem decay of organic matter, the peloids features remained, surrounded by spar cement or not (Kazmierczak *et al.*, 1996). Although we do not interpret micrite formation as calcification of the cells themselves, decay of non-mineralized EPS may be the process of peloidal micrite formation inside restricted pockets with precipitated micrite.

The isotopic values show an overall 13C enriched, suggesting high levels of photoautotroph carbon fixation (Burne and Moore, 1987; Pentecost and Spiro, 1990; Schidlowski, 2000) in agreement with carbonate precipitation by cyanobacteria. The end members of the micrite and microsparite isotopic values show enrichment of $\delta^{13}C$. Micrite is slightly (>4.5‰ VPDB) heavier than microsparite (<3.5‰ VPDB), suggesting that micrite is more closely associated with photoautotrophs than microsparite.

Our findings, then, suggest that microfabrics are captions of different bio-induced, bio-influenced processes (*sensu* Dupraz *et al.*, 2009) and stages of mineralization in the distinct microdomains within the microbial mat (*sensu* Decho, 2000). Following the findings of Kuhl *et al.* (2003; and references therein) and Kazmierczak *et al.* (2015), these domains would be of different viscosities, with possible different dominant metabolic type bacteria, resulting in microenvironmental gradients. The sticky cyanobacteria domains (since they trapped grains) possibly created the conditions for the early mineralization by Mg-Ca-nanospheres. Other microdomains were probably dominated by other bacteria types, such as heterotrophic. The occurrence of microlaminations (LM) and pockets (MM, PM) next to diffuse microfabrics (CM, MM) may reflect segregations inside microbial mat and processes of degradation.

5.3 MODEL OF MINERALIZATION

As argued above, the exact nature of the precipitation is quite hard to define without microbiological data. We, thus, suggest that microbialite lithification within Laguna del Toro could have occurred as summarized: (1) The microbial mats with distinctive microenvironments established at the bottom of the lake; (2) Some of these

domains were early permineralized by photosynthetic CO_2 uptake and alkalinity enhance; (4) The non-mineralized EPS were degraded, either by heterotrophic consumption, UV exposure, changes in the environment (seasonal fluctuations, water energy and etc.); (5) Degradation was followed by precipitation of calcite (microsparite), in the first moment, forming extensive microsparitic domains; (6) The continuity of degradation led to the shrinkage of cyanobacteria-dominated biofilm, releasing the bound Ca^{2+} and Mg^{2+} precipitating Clotted micrite and Mixed micrite-microsparite; (7) In the opened space, calcification could occur by physicochemical processes forming microsparite; (8) Inside the micritic domains continued mineralization and organic matter decay would led to the formation of the pockets of Peloidal micrite; (9) Decay of organic matter may have left opened spaces forming the vugs and fenestrae (as traces of organic matter-rich micrite occur on the porosity walls, Fig. 7H); (10) Post-lithified, localized, carbonate neoformation occurred in the pores walls, and the vugs were sedimented (Geopetal microfabrics).

5.4 BUILD-UP GROWTH AND PALEOENVIRONMENTAL IMPLICATIONS

The modern Laguna del Toro physiochemical characteristics and the microfabrics discussed above indicate that the paleolake was an alkaline/saline system. Not only do the inferred precipitation processes indicate that, but the preservation of the filamentous bacteria which require high $CaCO_3$ saturation states (Merz, 1992; Aloisi, 2008).

We found two different morphologies, that however show the same fabrics. It indicates that growth morphologies were rather a product of distinct environment conditionings than distinct lithification processes. The mounds form beds of laterally linked heads at the base and inner parts of deposits. The pinnacles grew over the mounds and occur farther from the modern lake. To pinnacles grow they need accommodation space, water, cation availability, microbial community, and energy (Baskin, 2014). The energy of the system was registered by the occurrence of 3 types of oolites and detrital grains, distributed not equally along with the build-ups. Indicating, not only, that build-ups grew above the wave-sediment interface, but variations in the paleoenvironment energy. Thus, we interpret that the water level to form the pinnacles needed to be at least 3 meters higher than the paleo level of mound formation, based on pinnacles height and the altitude of the farther carbonate crusts found.

Thus, it is possible that the lake level rose to create accommodation space and force the build-ups to grow upward following the light, resulting in the pinnacles. Studies of quaternary mounds and pinnacles, like Mono Lake (Brasier *et al.*, 2018), Lake Van (Kempe *et al.*, 1991; Kremer *et al.*, 2019), and Searles Lake (Guo and Chafetz, 2012), have shown that these structures have been formed by microbial communities in groundwater-discharge zones (sub-lacustrine tufa, in Jones and Renaut, 2010). In particular, Della Porta (2015) and Warden *et al.* (2019) suggested the importance of groundwater flow to the formation of thrombolite mesostructure itself. It is a possibility to have happened in Laguna del Toro, due to the morphology and occurrence of N-NNW aligned clusters of pinnacles. The clustered pinnacles contrast with the smaller and dispersed pinnacles at the eastern margin. Such differentiation in occurrence could be by differences in wave energy (today it is bigger at the southwestern facing shores) or structures below the lake. It would also be in agreement with the possibility of precipitation only being allowed by high Ca^{2+} and Mg^{2+} and low DIC fluids discharging into the alkaline lake.

Our bulk-rock oxygen isotopes results (-2.7 to -0.03‰ VPDB) only indicate that the formation water was concordant to the rain in coastal-to-continental (early Rayleigh fractionation), which matches with the probable rain signals for this region in the Holocene. The $\delta^{18}O$ (-2.51 to -1.73‰ VPDB) and $\delta^{13}C$ (1.55-2.16‰ VPDB) values of the top of pinnacles (tufa facies) and their textures indicate that, at some point, the structures were at the water-air interface and carbonate precipitation occurred by CO_2 degassing.

Although morphologies and structures distributions indicate meter-high water level fluctuations, further investigation is needed to evaluate the evolution of the lake during the Holocene. Moreover, the nature of these fluctuations, if related to marine transgressions, climate variations, or discharge of a large amount of groundwater.

5.5 GEOLOGIC RECORD IMPLICATIONS

Several studies have described massive, patchy, and peloidal micrite in ancient rocks, mostly from Neoproterozoic (*e.g.*, Aitken,1967; Aitken and Narbonne, 1989; Pratt, 1995; Grotzinger and James, 2000; Turner *et al.*, 2000; Hardwood and Sumner, 2012) to the Paleozoic (*e.g.*, Pratt and James, 1982; Guo and Riding, 1992; Armella, 1994; Kennard and James, 1996; Kahle, 2001; Stephens and Sumner, 2002). These papers often highlight the difficulty to determine the origin and environmental

significance of mesoclots or specific microstructures (*e.g.*, Kahle, 2001; Hardwood and Sumner, 2012), since these rocks have their (bio)structures obliterated by successive diagenetic processes.

We showed the relation between micrite, EPS, and cyanobacteria occurrence in contrast to microsparite, and proposed possible paths for microbial growth and microbial lithification in microbialites within Laguna del Toro. Thus, petrographic features shown in this paper can help identify and interpret the fabrics of ancient rocks. Moreover, microfabrics can serve as proxies for the cold, continental, alkaline-lacustrine environment, once they not only indicate biologic intrinsic factors but often its environmental conditioners (Suarez-Gonzalez *et al.*, 2019).

The unique morphologies of the carbonate deposits are analogs candidates to similar structures in the geologic record. Recent studies have been discussed the origin of pinnacles and mounds morphologies in ancient rocks units (*e.g.*, Awramik and Buchheim, 2015; Alonso-Zarza *et al.*, 2020; Baddouh *et al.*, 2021; Jagniecki *et al.*, 2021). Thus, our findings can provide insights into microbial importance on the build-up growth of these ancient analogs.

6 CONCLUSION

The extensive mounds and pinnacles carbonate deposits within Laguna del Toro are interpreted to be formed by the interplay of complex bio-influenced and bio-induced processes inside a microbial community. The microfabrics registries the different processes and stages of EPS mineralization, degradation, and physicochemical carbonate precipitation processes associated.

Mineralization of EPS was led by cyanobacteria photosynthetic activity and is recorded in the massive, peloidal micrite and micrite laminae. The EPS degradation led to the precipitation of diffuse fabrics, such as clotted micrite and mixed micrite-microsparite. Microsparite formation seems to be related to distinct microdomains other than the cyanobacteria-dominated and with degradation of these domains. These processes occurred successively along with the paleolake environmental variations in the Holocene. Distinct mound and pinnacles morphologies were formed by similar processes within microbial communities. The onset of changes in the paleolake (water-level variations) possibly led to the morphology variation from the mounds to pinnacles. Later lakeshore regression exposed most of these carbonate deposits and possibly

was followed by changes that altered the physiochemical conditions which inhibited the formation of lithifying microbial mats in the present.

The good petrography preservation of these rocks makes them suitable to provide insights into the formation of frequent microstructures in non-laminated microbialites of the geologic record (*e.g.*, "clotted" or "patchy micrite", "peloids", "aphanitic micrite" and "filamentous fabrics"). Moreover, the mineralogical to morphological aspects can serve as proxies to identifying similar environments on ancient carbonate deposits.

Further investigations will provide a better understanding of the microbial composition and paleoenvironmental conditions for microbialite growth and lithification.

5 CONSIDERAÇÕES FINAIS

A investigação em múltipla escala de microbialitos, aliada ao uso de isótopos estáveis, forneceu importantes informações acerca de estruturas tipicamente encontradas em microbialitos do registro geológico. Deste modo, a *Laguna del Toro* se coloca como interessante análogo para o entendimento da gênese e importância biológica e paleoambiental dessas estruturas no registro geológico. Além disso, o caráter inédito do estudo se mostra importante para o entendimento da evolução geológica, climática, morfológica e tectônica da região de *Magallanes* durante o Quaternário tardio.

Os depósitos de microbialitos sub-fósseis expostos nas margens da *Laguna del Toro* mostram duas distintas feições morfológicas, formadas pela mesma assembleia de microfábricas. Estas, por sua vez, são registros de uma comunidade microbiana provavelmente formada por diversos micro-domínios, caracterizados por distintas propriedades físico-químicas e biológicas. As distintas microfábricas são produtos da mineralização e degradação de EPS e precipitação carbonática físico-química. Resultando em uma grande complexidade textural e mineralógica entre as microfábricas. A identificação mineralógica feita aqui é de caráter preliminar, mas permitiu interpretar as possíveis ocorrências de cada fase e seu modo de precipitação. Recomenda-se, no entanto, um estudo aprofundado para melhor caracterização mineralógica qualitativa e quantitativa, possibilitando melhor entendimento da ocorrência das fases minerais pouco comuns em ambiente naturais modernos, como a monohidrocalcita e dolomita.

Os dados de isótopos de carbono e oxigênio foram primordiais no refinamento da interpretação de processos de precipitação, bem como, do paleoambiente. Com a construção de digramas de variação isotópica ao longo das estruturas microbiais (quimioestratigrafia; Apêndice 5) é possível realizar um estudo de evolução paleoambiental da região durante o Holoceno. Aliando estes dados a dados de isótopos de Sr, poderemos identificar as fontes de cátions e refinar o modelo paleoambiental e geoquímico quando da formação destes microbialitos. Trabalho este que fora realizado parcialmente durante este mestrado e que deve ser publicado futuramente.

REFERÊNCIAS

Aitken, J. D. (1967). Classification and environmental significance of cryptalgal limestones and dolomites, with illustrations from the Cambrian and Ordovician of southwestern Alberta. *Journal of Sedimentary Research*, *37*(4), 1163-1178.

Aitken, J. D., & Narbonne, G. M. (1989). Two occurrences of Precambrian thrombolites from the Mackenzie Mountains, northwestern Canada. *Palaios*, 384-388.

Aloisi, G. (2008). The calcium carbonate saturation state in cyanobacterial mats throughout Earth's history. *Geochimica et Cosmochimica Acta*, *72*(24), 6037-6060.

Alonso-Zarza, A. M., Cabaleri, N. G., Huerta, P., Armella, C., Rodríguez-Berriguete, Á., Monferran, M. D., ... & Nieto, D. S. (2020). Lacustrine microbialite pinnacles in the Palaeogene of Patagonia, Argentina: Facies and controls. *Sedimentary Geology*, *408*, 105742.

Armella, C. (1994). Thrombolitic-stromatolitic cycles of the Cambro-Ordovician boundary sequence, Precordillera Oriental Basin, western Argentina. In *Phanerozoic stromatolites II* (pp. 421-441). Springer, Dordrecht.

Arp, G., Reimer, A., & Reitner, J. (1999a). Calcification in cyanobacterial biofilms of alkaline salt lakes. *European Journal of Phycology*, *34*(4), 393-403.

Arp, G., Thiel, V., Reimer, A., Michaelis, W., & Reitner, J. (1999b). Biofilm exopolymers control microbialite formation at thermal springs discharging into the alkaline Pyramid Lake, Nevada, USA. *Sedimentary Geology*, *126*(1-4), 159-176.

Arp, G., Reimer, A., & Reitner, J. (2001). Photosynthesis-induced biofilm calcification and calcium concentrations in Phanerozoic oceans. *Science*, *292*(5522), 1701-1704.

Arp, G., Reimer, A., & Reitner, J. (2003). Microbialite formation in seawater of increased alkalinity, Satonda Crater Lake, Indonesia. *Journal of sedimentary research*, *73*(1), 105-127.

Awramik, S. M. (1971). Precambrian columnar stromatolite diversity: reflection of metazoan appearance. *Science*, *174*(4011), 825-827.

Awramik, S. M., & Buchheim, H. P. (2015). Giant stromatolites of the Eocene Green River Formation (Colorado, USA). *Geology*, *43*(8), 691-694.

Baddouh, M. B., Carroll, A. R., Jagniecki, E. A., Beard, B. L., Lowenstein, T. K., & Johnson, C. M. (2021). Groundwater mixing in an alkaline paleolake: Eocene Green River Formation, Wyoming. *Palaeogeography, Palaeoclimatology, Palaeoecology*, *561*, 110038.

Baskin, R. L. (2014). *OCCURRENCE AND SPATIAL DISTRIBUTION OF MICROBIAL BIOHERMS IN* (Doctoral dissertation, The University of Utah).

Benn, D. I., & Clapperton, C. M. (2000). Glacial sediment–landform associations and paleoclimate during the last glaciation, Strait of Magellan, Chile. *Quaternary Research*, *54*(1), 13-23.

Bischoff, J. L., Stine, S., Rosenbauer, R. J., Fitzpatrick, J. A., & Stafford Jr, T. W. (1993). Ikaite precipitation by mixing of shoreline springs and lake water, Mono Lake, California, USA. *Geochimica et cosmochimica acta*, *57*(16), 3855-3865.

Bischoff, K., Sirantoine, E., Wilson, M. E., George, A. D., Mendes Monteiro, J., & Saunders, M. (2020). Spherulitic microbialites from modern hypersaline lakes, Rottnest Island, Western Australia. *Geobiology*, *18*(6), 725-741.

Bosence, D., & Gallois, A. (2021). How do thrombolites form? Multiphase construction of lacustrine microbialites, Purbeck Limestone Group, (Jurassic), Dorset, UK. *Sedimentology*.

Brasier, A., Wacey, D., Rogerson, M., Guagliardo, P., Saunders, M., Kellner, S., ... & Reijmer, J. (2018). A microbial role in the construction of Mono Lake carbonate chimneys? *Geobiology*, *16*(5), 540-555.

Breitsprecher, K., & Thorkelson, D. J. (2009). Neogene kinematic history of Nazca–Antarctic–Phoenix slab windows beneath Patagonia and the Antarctic Peninsula. *Tectonophysics*, *464*(1-4), 10-20.

Burne, R. V., & Moore, L. S. (1987). Microbialites; organosedimentary deposits of benthic microbial communities. *Palaios*, *2*(3), 241-254.

Burne, R. V., Moore, L. S., Christy, A. G., Troitzsch, U., King, P. L., Carnerup, A. M., & Hamilton, P. J. (2014). Stevensite in the modern thrombolites of Lake Clifton, Western Australia: A missing link in microbialite mineralization? *Geology*, *42*(7), 575-578.

Carrasco, J. F., Casassa, G., & Rivera, A. (2002). Meteorological and climatological aspects of the Southern Patagonia Icefield. In *The Patagonian Icefields* (pp. 29-41). Springer, Boston, MA.

Chagas, A. A., Webb, G. E., Burne, R. V., & Southam, G. (2016). Modern lacustrine microbialites: towards a synthesis of aqueous and carbonate geochemistry and mineralogy. *Earth-Science Reviews*, *162*, 338-363.

Clapperton, C. M., Sugden, D. E., Kaufman, D. S., & McCulloch, R. D. (1995). The last glaciation in central Magellan Strait, southernmost Chile. *Quaternary Research*, *44*(2), 133-148.

Couradeau, E., Benzerara, K., Gérard, E., Estève, I., Moreira, D., Tavera, R., & López-García, P. (2013). Cyanobacterial calcification in modern microbialites at the submicrometer scale. *Biogeosciences*, *10*(8), 5255-5266.

Coronato, A. M., Coronato, F., Mazzoni, E., & Vázquez, M. (2008). The physical geography of Patagonia and Tierra del Fuego. *Developments in Quaternary Sciences*, *11*, 13-55.

Dahl, K., & Buchardt, B. (2006). Monohydrocalcite in the arctic Ikka fjord, SW Greenland: first reported marine occurrence. *Journal of Sedimentary Research*, *76*(3), 460-471.

Darvill, C. M., Bentley, M. J., Stokes, C. R., Hein, A. S., & Rodés, Á. (2015). Extensive MIS 3 glaciation in southernmost Patagonia revealed by cosmogenic nuclide dating of outwash sediments. *Earth and Planetary Science Letters*, *429*, 157-169.

Davies, B. J., Darvill, C. M., Lovell, H., Bendle, J. M., Dowdeswell, J. A., Fabel, D., ... & Thorndycraft, V. R. (2020). The evolution of the Patagonian Ice Sheet from 35 ka to the present day (PATICE). *Earth-Science Reviews*, *204*, 103152.

Decho, A. W. (2000). Exopolymer microdomains as a structuring agent for heterogeneity within microbial biofilms. In *Microbial sediments* (pp. 9-15). Springer, Berlin, Heidelberg.

DeFarge, C., Trichet, J., Jaunet, A. M., Robert, M., Tribble, J., & Sansone, F. J. (1996). Texture of microbial sediments revealed by cryo-scanning electron microscopy. *Journal of Sedimentary Research*, *66*(5), 935-947.

Della Porta, G. (2015). Carbonate build-ups in lacustrine, hydrothermal and fluvial settings: comparing depositional geometry, fabric types and geochemical signature. *Geological Society, London, Special Publications*, *418*(1), 17-68.

Diraison, M., Cobbold, P. R., Gapais, D., & Rossello, E. A. (1997). Magellan Strait: part of a Neogene rift system. *Geology*, *25*(8), 703-706.

Diraison, M., Cobbold, P. R., Gapais, D., Rossello, E. A., & Le Corre, C. (2000). Cenozoic crustal thickening, wrenching and rifting in the foothills of the southernmost Andes. *Tectonophysics*, *316*(1-2), 91-119.

Dupraz, C., Visscher, P. T., Baumgartner, L. K., & Reid, R. P. (2004). Microbe–mineral interactions: early carbonate precipitation in a hypersaline lake (Eleuthera Island, Bahamas). *Sedimentology*, *51*(4), 745-765.

Dupraz, C., & Visscher, P. T. (2005). Microbial lithification in marine stromatolites and hypersaline mats. *Trends in microbiology*, *13*(9), 429-438.

Dupraz, C., Reid, R. P., Braissant, O., Decho, A. W., Norman, R. S., & Visscher, P. T. (2009). Processes of carbonate precipitation in modern microbial mats. *Earth-Science Reviews*, *96*(3), 141-162.

Dupraz, C., Reid, R. P., Visscher, P. T., Reitner, J., & Thiel, V. (2011). Microbialites, modern. *Encyclopedia of geobiology*, 617-635.

Fildani, A., Romans, B. W., Fosdick, J. C., Crane, W. H., & Hubbard, S. M. (2008). Orogenesis of the Patagonian Andes as reflected by basin evolution in southernmost South America. *Arizona Geological Society Digest*, *22*, 259-268.

Fosdick, J. C., Romans, B. W., Fildani, A., Bernhardt, A., Calderón, M., & Graham, S. A. (2011). Kinematic evolution of the Patagonian retroarc fold-and-thrust belt

and Magallanes foreland basin, Chile and Argentina, 51 30′ S. *Bulletin*, *123*(9-10), 1679-1698.

Garreaud, R., Lopez, P., Minvielle, M., & Rojas, M. (2013). Large-scale control on the Patagonian climate. *Journal of Climate*, *26*(1), 215-230.

Ghiglione, M. C., Navarrete-Rodríguez, A. T., González-Guillot, M., & Bujalesky, G. (2013). The opening of the Magellan Strait and its geodynamic implications. *Terra Nova*, *25*(1), 13-20.

Golubic, S., & Hofmann, H. J. (1976). Comparison of Holocene and mid-Precambrian Entophysalidaceae (Cyanophyta) in stromatolitic algal mats: cell division and degradation. *Journal of Paleontology*, 1074-1082.

González, E. (1965). La cuenca petrolífera de Magallanes. Instituto de Ingenieros de Minas de Chile. *Revista Minerales*, *20*(91), 43-61.

Grotzinger, J. P., & Knoll, A. H. (1999). Stromatolites in Precambrian carbonates: evolutionary mileposts or environmental dipsticks?.*Annual review of earth and planetary sciences*, *27*(1), 313-358.

Grotzinger, J. P., & James, N. P. (2000). Precambrian carbonates: evolution of understanding.

Guo, L., & Riding, R. (1992). Microbial micritic carbonates in uppermost Permian reefs, Sichuan Basin, southern China: some similarities with Recent travertines. *Sedimentology*, *39*(1), 37-53.

Guo, X., & Chafetz, H. S. (2012). Large tufa mounds, Searles Lake, California. *Sedimentology*, *59*(5), 1509-1535.

Harada, N., Ninnemann, U., Lange, C. B., Marchant, M. E., Sato, M., Ahagon, N., & Pantoja, S. (2013). Deglacial–Holocene environmental changes at the Pacific entrance of the Strait of Magellan. *Palaeogeography, Palaeoclimatology, Palaeoecology*, *375*, 125-135.

Harwood, C. L., & Sumner, D. Y. (2012). Origins of microbial microstructures in the Neoproterozoic Beck Spring Dolomite: variations in microbial community and timing of lithification. *Journal of Sedimentary Research*, *82*(9), 709-722.

Hofmann, H. J., Grey, K., Hickman, A. H., & Thorpe, R. I. (1999). Origin of 3.45 Ga coniform stromatolites in Warrawoona group, Western Australia. *Geological Society of America Bulletin*, *111*(8), 1256-1262.

Jagniecki, E. A., Lowenstein, T. K., Demicco, R. V., Baddouh, M. B., Carroll, A. R., Beard, B. L., & Johnson, C. M. (2021). Spring origin of Eocene carbonate mounds in the Green River Formation, Northern Bridger Basin, Wyoming, USA. *Sedimentology*, *68*(6), 2334-2364.

Jones, B., & Renaut, R. W. (2010). Calcareous spring deposits in continental settings. *Developments in Sedimentology*, *61*, 177-224.

Kahle, C. F. (2001). Biosedimentology of a Silurian thrombolite reef with meter-scale growth framework cavities. *Journal of Sedimentary Research*, *71*(3), 410-422.

Kalkowsky, E. (1908). Oolith und Stromatolith im norddeutschen Buntsandstein. *Zeitschrift der deutschen geologischen Gesellschaft*, 68-125.

Kazmierczak, J., Coleman, M. L., Gruszczynski, M., & Kempe, S. (1996). Cyanobacterial key to the genesis of micritic and peloidal limestones in ancient seas. *Acta Palaeontologica Polonica*, *41*(4), 319-338.

Kaźmierczak, J., Fenchel, T., Kühl, M., Kempe, S., Kremer, B., Łącka, B., & Małkowski, K. (2015). CaCO3 precipitation in multilayered cyanobacterial mats: clues to explain the alternation of micrite and sparite layers in calcareous stromatolites. *Life*, *5*(1), 744-769.

Kempe, S., Kazmierczak, J., Landmann, G., Konuk, T., Reimer, A., & Lipp, A. (1991). Largest known microbialites discovered in Lake Van, Turkey. *Nature*, *349*(6310), 605-608.

Kennard, J. M., & James, N. P. (1986). Thrombolites and stromatolites: two distinct types of microbial structures. *Palaios*, 492-503.

Kilian, R., & Lamy, F. (2012). A review of Glacial and Holocene paleoclimate records from southernmost Patagonia (49–55 S). *Quaternary Science Reviews*, *53*, 1-23.

Kilian, R., Baeza, O., Breuer, S., Ríos, F., Arz, H., Lamy, F., Wirtz, J., Baque, D., Korf, P., Kremer, K., Ríos, C., Mutschke, E., Simon, M., De Pol-Holz, R., Arevalo, M., Wörner, G., Schneider, C. & Casassa, G. (2013). Late Glacial and Holocene paleogeographical and paleoecological evolution of the Seno Skyring and Otway fjord systems in the Magellan region. Anales Instituto Patagonia (Chile), 41(2), 5-26.

Kitajima, T., Fukushi, K., Yoda, M., Takeichi, Y., & Takahashi, Y. (2020). Simple, reproducible synthesis of pure monohydrocalcite with low Mg content. *Minerals*, *10*(4), 346.

Kremer, B., Kaźmierczak, J., & Kempe, S. (2019). Authigenic replacement of cyanobacterially precipitated calcium carbonate by aluminium-silicates in giant microbialites of Lake Van (Turkey). *Sedimentology*, *66*(1), 285-304.

Kühl, M., Fenchel, T., & Kazmierczak, J. (2003). Growth, structure and calcification potential of an artificial cyanobacterial mat. In *Fossil and recent biofilms* (pp. 77-102). Springer, Dordrecht.

Li, M., Kang, S., Zhu, L., You, Q., Zhang, Q., & Wang, J. (2008). Mineralogy and geochemistry of the Holocene lacustrine sediments in Nam Co, Tibet. *Quaternary International*, *187*(1), 105-116.

Lin, C. Y., Turchyn, A. V., Steiner, Z., Bots, P., Lampronti, G. I., & Tosca, N. J. (2018). The role of microbial sulfate reduction in calcium carbonate polymorph selection. *Geochimica et Cosmochimica Acta*, *237*, 184-204.

Ludwig, R., Al-Horani, F. A., De Beer, D., & Jonkers, H. M. (2005). Photosynthesis-controlled calcification in a hypersaline microbial mat. *Limnology and Oceanography*, *50*(6), 1836-1843.

Mazzarini, F., & D'Orazio, M. (2003). Spatial distribution of cones and satellite-detected lineaments in the Pali Aike Volcanic Field (southernmost Patagonia): insights into the tectonic setting of a Neogene rift system. *Journal of Volcanology and Geothermal Research*, *125*(3-4), 291-305.

Mcculloch, R. D., & Bentley, M. J. (1998). Late glacial ice advances in the Strait of Magellan, southern Chile. *Quaternary Science Reviews*, *17*(8), 775-787.

McCulloch, R. D., Fogwill, C. J., Sugden, D. E., Bentley, M. J., & Kubik, P. W. (2005). Chronology of the last glaciation in central Strait of Magellan and Bahía Inútil, southernmost South America. *Geografiska Annaler: Series A, Physical Geography*, *87*(2), 289-312.

Merz, M. U. (1992). The biology of carbonate precipitation by cyanobacteria. *Facies*, *26*(1), 81-101.

Merz-Preiß, M., & Riding, R. (1999). Cyanobacterial tufa calcification in two freshwater streams: ambient environment, chemical thresholds and biological processes. *Sedimentary Geology*, *126*(1-4), 103-124.

Merz-Preiß, M. (2000). Calcification in cyanobacteria. In *Microbial sediments* (pp. 50-56). Springer, Berlin, Heidelberg.

Mucci, A., Canuel, R., & Zhong, S. (1989). The solubility of calcite and aragonite in sulfate-free seawater and the seeded growth kinetics and composition of the precipitates at 25 C. *Chemical geology*, *74*(3-4), 309-320.

Nielsen, M. R., Sand, K. K., Rodriguez-Blanco, J. D., Bovet, N., Generosi, J., Dalby, K. N., & Stipp, S. L. S. (2016). Inhibition of calcite growth: combined effects of Mg2+ and SO42–. *Crystal Growth & Design*, *16*(11), 6199-6207.

Oehlerich, M., Mayr, C., Griesshaber, E., Lücke, A., Oeckler, O. M., Ohlendorf, C., ... & Zolitschka, B. (2013). Ikaite precipitation in a lacustrine environment–implications for palaeoclimatic studies using carbonates from Laguna Potrok Aike (Patagonia, Argentina). *Quaternary Science Reviews*, *71*, 46-53.

Pan, J., Zhao, H., Tucker, M. E., Zhou, J., Jiang, M., Wang, Y., ... & Yan, H. (2019). Biomineralization of monohydrocalcite induced by the halophile Halomonas smyrnensis WMS-3. *Minerals*, *9*(10), 632.

Parkhurst, D. L., Thorstenson, D. C., & Plummer, L. N. (1982). *PHREEQE: A computer program for geochemical calculations* (Vol. 80). US Geological Survey, Water Resources Division.

Párraga, J., Rivadeneyra, M. A., Delgado, R., Iniguez, J., Soriano, M., & Delgado, G. (1998). Study of biomineral formation by bacteria from soil solution equilibria. *Reactive and Functional Polymers*, *36*(3), 265-271.

Pentecost, A., & Spiro, B. (1990). Stable carbon and oxygen isotope composition of calcites associated with modern freshwater cyanobacteria and algae. *Geomicrobiology Journal*, *8*(1), 17-26.

Perri, E., Tucker, M. E., & Spadafora, A. (2012). Carbonate organo-mineral micro-and ultrastructures in sub-fossil stromatolites: Marion lake, South Australia. *Geobiology*, *10*(2), 105-117.

Pratt, B. R., & James, N. P. (1982). Cryptalgal-metazoan bioherms of early Ordovician age in the St George Group, western Newfoundland. *Sedimentology*, *29*(4), 543-569.

Pratt, B. R. (1984). Epiphyton and Renalcis; diagenetic microfossils from calcification of coccoid blue-green algae. *Journal of Sedimentary Research*, *54*(3), 948-971.

Ramos, V. A. (1989). Andean foothills structures in northern Magallanes Basin, Argentina. *AAPG bulletin*, *73*(7), 887-903.

Ramos, V. A., & Kay, S. M. (1992). Southern Patagonian plateau basalts and deformation: backarc testimony of ridge collisions. *Tectonophysics*, *205*(1-3), 261-282.

Riding, R., Braga, J. C., & Martin, J. M. (1991). Oolite stromatolites and thrombolites, Miocene, Spain: analogues of Recent giant Bahamian examples. *Sedimentary Geology*, *71*(3-4), 121-127.

Riding, R. (1991). Classification of microbial carbonates. In *Calcareous algae and stromatolites* (pp. 21-51). Springer, Berlin, Heidelberg.

Riding, R. (2000). Microbial carbonates: the geological record of calcified bacterial–algal mats and biofilms. *Sedimentology*, *47*, 179-214.

Riding, R., & Tomás, S. (2006). Stromatolite reef crusts, Early Cretaceous, Spain: bacterial origin of in situ-precipitated peloid microspar? *Sedimentology*, *53*(1), 23-34.

Riding, R. (2011a). Microbialites, stromatolites, and thrombolites. In *Encyclopedia of geobiology*.

Riding, R. (2011b). The nature of stromatolites: 3,500 million years of history and a century of research. In *Advances in stromatolite geobiology* (pp. 29-74). Springer, Berlin, Heidelberg.

Rodriguez-Blanco, J. D., Shaw, S., Bots, P., Roncal-Herrero, T., & Benning, L. G. (2014). The role of Mg in the crystallization of monohydrocalcite. *Geochimica et Cosmochimica Acta*, *127*, 204-220.

Schidlowski, M. (2000). Carbon isotopes and microbial sediments. In *Microbial sediments* (pp. 84-95). Springer, Berlin, Heidelberg.

Sergeev, V. N., Gerasimenko, L. M., & Zavarzin, G. A. (2002). The proterozoic history and present state of cyanobacteria. *Microbiology*, *71*(6), 623-637.

Shapiro, R. S., & Awramik, S. M. (2000). Microbialite morphostratigraphy as a tool for correlating Late Cambrian–Early Ordovician sequences. *The Journal of Geology*, *108*(2), 171-180.

Shapiro, R. S. (2004). Neoproterozoic-Cambrian microbialite record. *The Paleontological Society Papers*, *10*, 5-16.

Shiraishi, F. (2012). Chemical conditions favoring photosynthesis-induced CaCO3 precipitation and implications for microbial carbonate formation in the ancient ocean. *Geochimica et Cosmochimica Acta*, *77*, 157-174.

Solotchina, E. P., Prokopenko, A. A., Kuzmin, M. I., Solotchin, P. A., & Zhdanova, A. N. (2009). Climate signals in sediment mineralogy of Lake Baikal and Lake Hovsgol during the LGM-Holocene transition and the 1-Ma carbonate record from the HDP-04 drill core. *Quaternary International*, *205*(1-2), 38-52.

Spadafora, A., Perri, E., McKenzie, J. A., & Vasconcelos, C. (2010). Microbial biomineralization processes forming modern Ca: Mg carbonate stromatolites. *Sedimentology*, *57*(1), 27-40.

Sprachta, S., Camoin, G., Golubic, S., & Le Campion, T. (2001). Microbialites in a modern lagoonal environment: nature and distribution, Tikehau atoll (French Polynesia). *Palaeogeography, Palaeoclimatology, Palaeoecology*, *175*(1-4), 103-124.

Stephens, N. P., & Sumner, D. Y. (2002). Renalcids as fossilized biofilm clusters. *Palaios*, *17*(3), 225-236.

Suarez-Gonzalez, P., Benito, M. I., Quijada, I. E., Mas, R., & Campos-Soto, S. (2019). 'Trapping and binding': A review of the factors controlling the development of fossil agglutinated microbialites and their distribution in space and time. *Earth-Science Reviews*, *194*, 182-215.

Theisen, C. H., Sumner, D. Y., Mackey, T. J., Lim, D. S. S., Brady, A. L., & Slater, G. F. (2015). Carbonate fabrics in the modern microbialites of Pavilion Lake: two suites of microfabrics that reflect variation in microbial community morphology, growth habit, and lithification. *Geobiology*, *13*(4), 357-372.

Turner, E. C., James, N. P., & Narbonne, G. M. (2000). Taphonomic control on microstructure in Early Neoproterozoic reefal stromatolites and thrombolites. *Palaios*, *15*(2), 87-111.

Van Lith, Y., Warthmann, R., Vasconcelos, C., & McKenzie, J. A. (2003). Microbial fossilization in carbonate sediments: a result of the bacterial surface involvement in dolomite precipitation. *Sedimentology*, *50*(2), 237-245.

Vasconcelos, C., McKenzie, J. A., Bernasconi, S., Grujic, D., & Tiens, A. J. (1995). Microbial mediation as a possible mechanism for natural dolomite formation at low temperatures. *Nature*, *377*(6546), 220-222.

Vereshchagin, O. S., Frank-Kamenetskaya, O. V., Kuz'mina, M. A., Chernyshova, I. A., & Shilovskikh, V. V. (2021). Effect of magnesium on monohydrocalcite

formation and unit-cell parameters. *American Mineralogist: Journal of Earth and Planetary Materials*, *106*(8), 1294-1305.

Walter, M. R., & Heys, G. R. (1985). Links between the rise of the metazoa and the decline of stromatolites. *Precambrian Research*, *29*(1-3), 149-174.

Warden, J. G., Coshell, L., Rosen, M. R., Breecker, D. O., Ruthrof, K. X., & Omelon, C. R. (2019). The importance of groundwater flow to the formation of modern thrombolitic microbialites. *Geobiology*, *17*(5), 536-550.

Zhang, F., Xu, H., Konishi, H., & Roden, E. E. (2010). A relationship between d 104 value and composition in the calcite-disordered dolomite solid-solution series. *American Mineralogist*, *95*(11-12), 1650-1656.

APÊNDICE 1 – DIAGRAMAS ESPECTRAIS (MEV-EDS) EXTRAS

1. MEV-BSE esparita

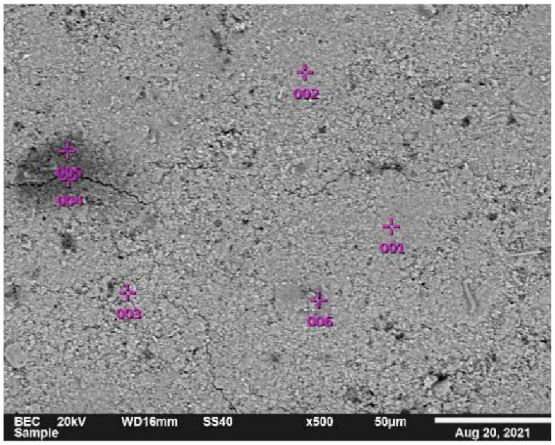

MEV-EDS diagramas elementais

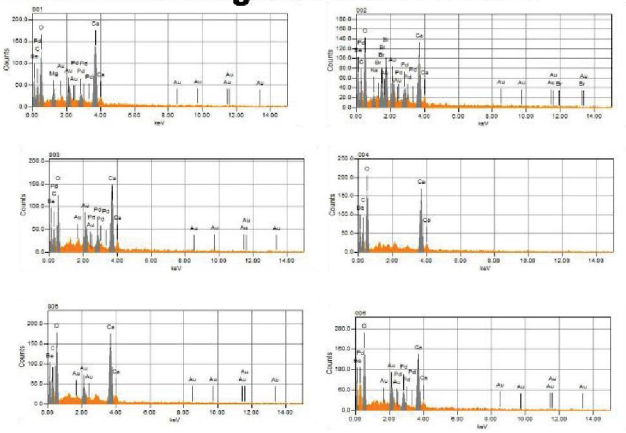

2. MEV-BSE micrita

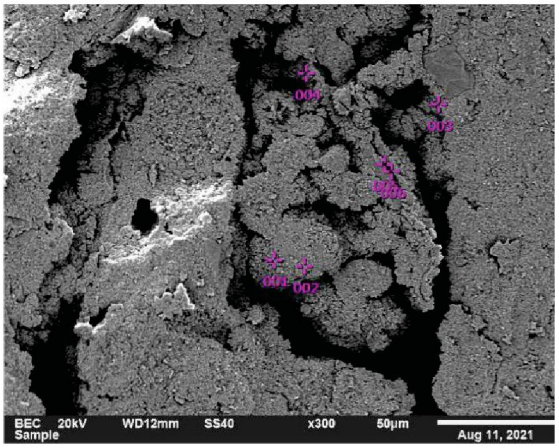

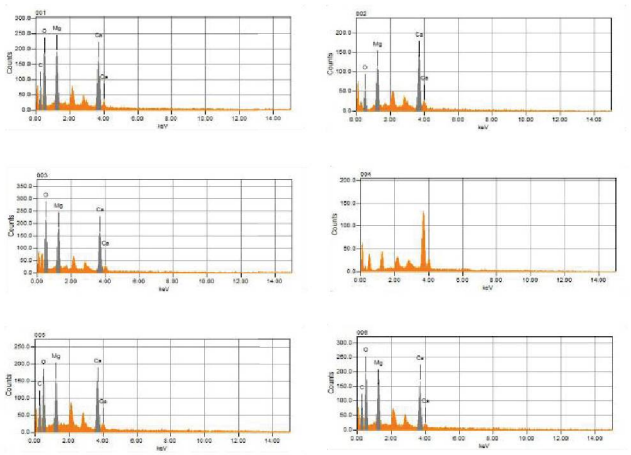

3. MEV-EDS Esparita e micrita

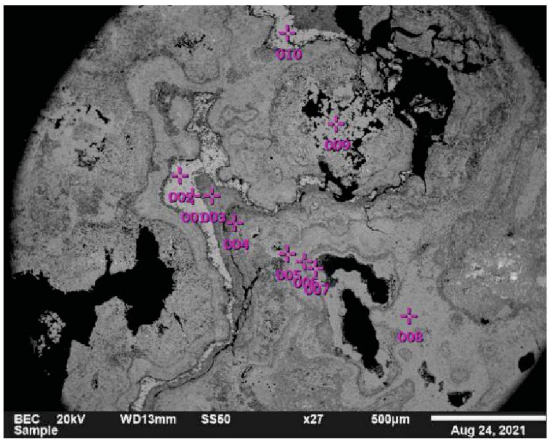

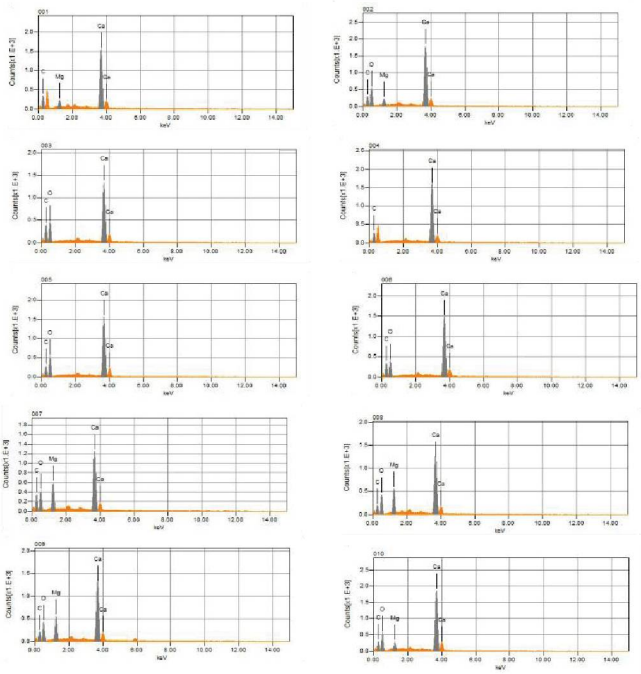

3. MEV-EDS Geopetal(silicatos detríticos em matriz micrítica)

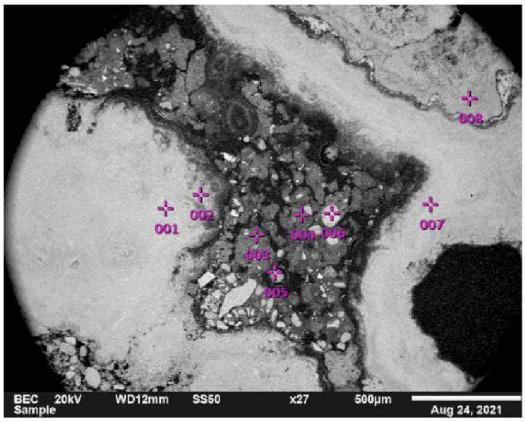

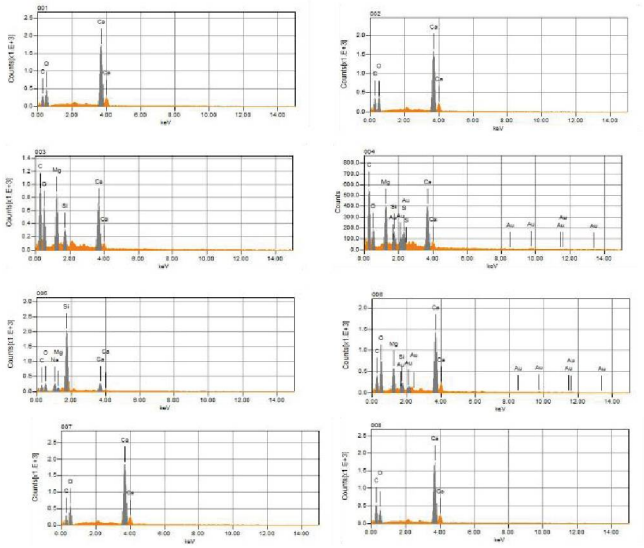

APÊNDICE 2 – MAPAS ELEMENTAIS (MEV-EDS) DE PORÇÃO MICRÍTICA COM MATÉRIA ORGÂNICA

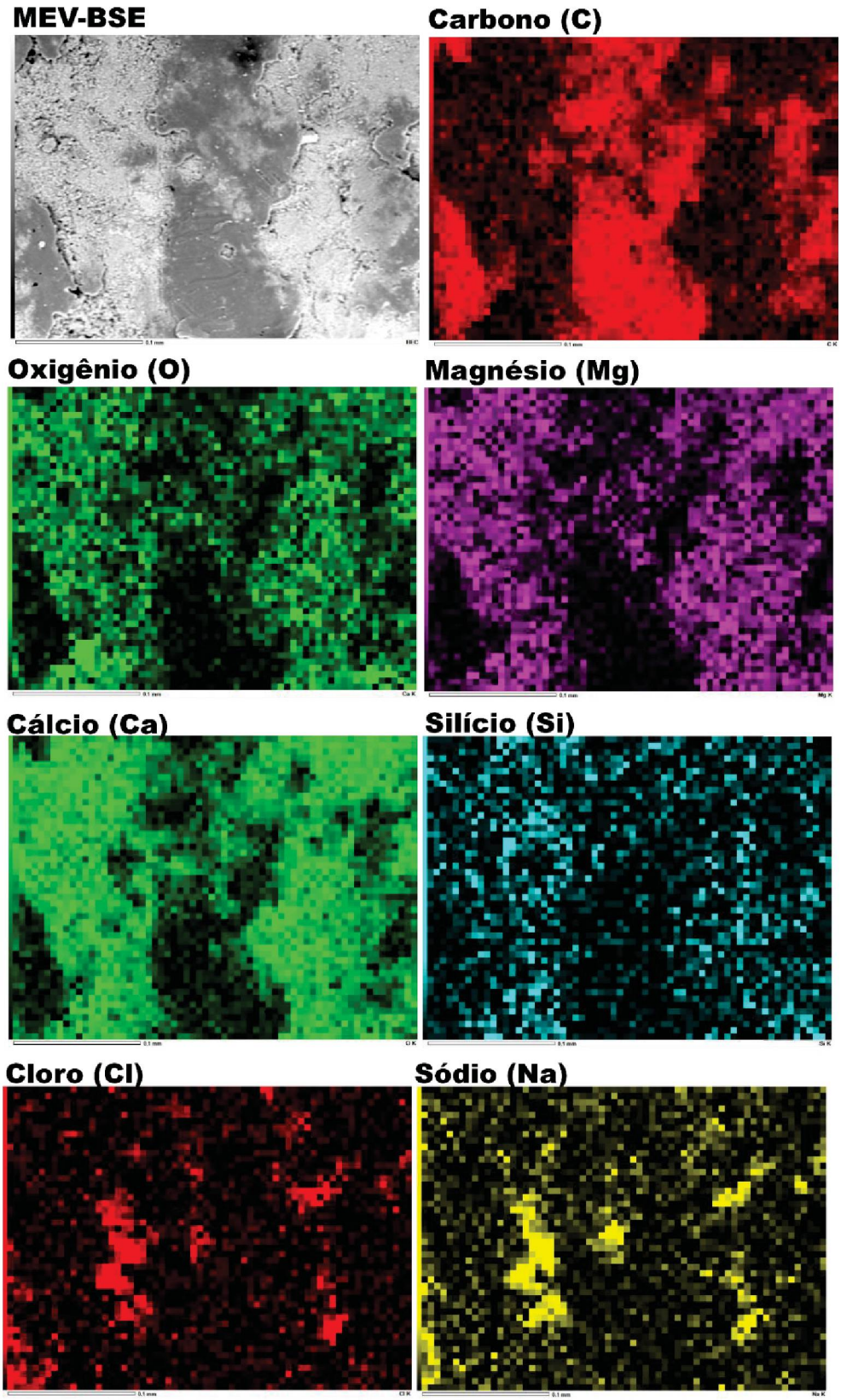

Legenda: Imagem de MEV-BSE de Micrita maciça, onde as porções claras são Mg-Ca-carbonatos e a porção cinza-escuro, matéria orgânica preservada (notar alto carbono na região).

APÊNDICE 3 – TABELA DADOS QUANTITATIVOS E QUALITATIVOS DO DRX

Sample	d-spacing (Å)				semi-quantitative (%)			
	MHC	Aragonite	Calcite	Dolomite	MHC	Aragonite	Calcite	Dolomite
TOR II A - 140	4.324	3.396	3.035	-	38	11	51	0
TOR II A - 80	-	3.396	3.035	2.909	0	85	4	11
TOR II A - 10	4.328	3.396	3.02	2.895	19	67	6	8
TOR IV A - topo	4.328	3.396	-	-	81	19	0	0
TOR IV A - meio	4.328	3.396	-	2.91	48	41	0	11
TOR IV A - base	4.328	3.396	-	-	88	12	0	0
TOR IV A - mound	4.328	3.396	3.035	2.89	40	17	28	16
TOR IV B - topo	4.328	-	3.036	-	89	0	11	0
TOR IV B - meio	4.328	3.396	-	2.915	12	80	0	8
TOR IV B - base	4.328	-	-	2.841	90	0	0	10
TOR VI A - topo	4.324	-	3.035	-	39	0	61	0
TOR VI A - meio	4.324	3.396	3.035	-	24	9	67	0
TOR VI A - base	4.324	3.395	3.02	2.915	23	25	43	9
TOR VI B - topo	-	-	3.035	2.91	0	0	75	25
TOR VI B - meio	4.328	3.395	-	-	89	11	0	0
TOR VI B - base	4.328	-	-	2.88	96	0	0	4
TOR VII A - topo	4.328	3.396	-	-	62	38	0	0
TOR VII A - meio	4.328	3.396	-	2.915	14	70	0	16
TOR VII A - base	4.328	3.396	-	2.911	40	34	0	26
TOR VII A - mound	4.328	-	-	2.911	54	0	0	46
	d-spacing (Å) mode				average (%)			
Total	4.328	3.396	3.035	2.915	47	26	17	9

APÊNDICE 4 – TABELA DADOS CARBONO E OXIGÊNIO

Amostra		$\delta^{13}C$ (‰ VPDB)	1σ [$\delta^{13}C$] (‰ VPDB)	$\delta^{18}O$ (‰ VPDB)	1σ [$\delta^{18}O$] (‰ VPDB)
Rocha-total	Pin1A	3.33	0.03	-0.49	0.07
	Pin1B	3.75	0.02	-0.76	0.05
	Pin1C	3.46	0.04	-1.17	0.04
	Pin1D	3.12	0.06	-1.54	0.06
	Pin1E	2.89	0.04	-1.54	0.07
	Pin1F	3.92	0.02	-1.09	0.05
	Pin1H	3.77	0.02	-1.04	0.04
	Pin1i	3.77	0.02	-1.34	0.04
	Pin1J	3.30	0.04	-1.53	0.04
	Pin1K	3.35	0.03	-1.99	0.05
	Pin1L	3.73	0.08	-1.43	0.04
	Pin1M	4.20	0.05	-0.98	0.04
	Pin1N	4.10	0.03	-1.05	0.04
	Pin1O	3.33	0.03	-1.41	0.04
	Pin1Q	3.77	0.08	-1.32	0.05
	Pin1R	3.76	0.03	-1.17	0.04
	Pin1S	3.95	0.05	-0.94	0.06
	Pin2A (crosta)	3.38	0.03	-1.44	0.05
	Pin2A	3.86	0.03	-0.74	0.04
	Pin2B	4.02	0.03	-1.24	0.06
	Pin2C	4.24	0.10	-0.95	0.04
	Pin2D	3.97	0.04	-1.20	0.03
	Pin2E	4.02	0.05	-1.10	0.07
	Pin2F	4.21	0.03	-0.86	0.07
	Pin2G	3.49	0.03	-1.53	0.04
	Pin2H	3.69	0.02	-1.33	0.03
	Pin2I	3.61	0.03	-1.46	0.04
	Pin2J	3.87	0.05	-1.09	0.05
	Pin2K	3.67	0.01	-1.44	0.05
	Pin2L	3.72	0.03	-1.30	0.06
	Pin2M	3.69	0.04	-1.38	0.04
	Pin2N	3.12	0.05	-1.84	0.06
	Pin2O	3.64	0.04	-0.93	0.04
	Pin2P	3.59	0.07	-1.36	0.05
	Pin2Q	3.69	0.09	-0.82	0.06
	TOR II A - 10	3.77	0.07	-0.91	0.04
	TOR II A - 20	3.94	0.05	-0.95	0.04
	TOR II A - 30	3.81	0.03	-0.80	0.03
	TOR II A - 40	4.26	0.08	-1.33	0.05
	TOR II A - 50	4.08	0.03	-1.40	0.03
	TOR II A - 60	3.55	0.04	-1.72	0.02

	TOR II A - 70	3.47	0.04	-2.77	0.03
	TOR II A - 80	4.46	0.10	-0.94	0.10
	TOR II A - 90	3.79	0.03	-1.38	0.03
	TOR II A - 100	3.37	0.04	-2.56	0.05
	TOR II A - 110	3.81	0.06	-1.22	0.09
	TOR II A - 120	4.08	0.08	-3.25	0.07
	TOR II A - 130	3.57	0.05	-2.69	0.05
	TOR II A - 140	3.68	0.08	-1.23	0.08
	TOR IV A - mound	3.43	0.04	-0.71	0.04
	TOR IV A - 15	3.94	0.04	-1.07	0.04
	TOR IV A - 25	4.10	0.03	-0.78	0.04
	TOR IV A - 35	4.39	0.06	-0.61	0.06
	TOR IV A - 45	4.00	0.10	-0.53	0.07
	TOR IV A - 55	3.85	0.05	-0.62	0.04
	TOR IV A - 65	4.26	0.03	-0.63	0.04
	TOR IV A - 75	4.07	0.10	-0.77	0.07
	TOR IV A - 85	4.30	0.03	-0.37	0.06
	TOR IV A - 95	3.98	0.04	-1.09	0.04
	TOR IV A - 105	4.13	0.03	-0.73	0.05
	TOR IV A - 115	4.44	0.03	-0.73	0.04
	TOR IV A - 125	3.88	0.03	-0.03	0.05
	TOR IV A - 135	3.76	0.03	-1.07	0.04
	TOR IV A - 145	3.98	0.05	-1.08	0.02
	TOR IV A - 155	4.00	0.03	-0.89	0.03
	TOR IV A - 165	4.02	0.08	-1.03	0.07
	TOR IV A - 175	4.02	0.03	-0.69	0.05
	TOR IV A - 185	4.09	0.10	-1.04	0.07
	TOR IV A - 195	3.99	0.02	-0.73	0.05
	TOR IV A - 205	4.01	0.03	-0.54	0.06
	TOR IV A - 215	4.08	0.10	-1.04	0.07
	TOR IV A - 225	3.72	0.06	-1.38	0.06
	TOR IV A - 235	3.77	0.07	-1.23	0.07
	TOR IV A - 245	4.26	0.04	-1.12	0.03
	TOR IV A - 255	4.40	0.07	-0.92	0.05
	TOR IV A - 265	3.24	0.02	-1.28	0.06
	TOR IV B - 15	3.96	0.02	-0.68	0.06
	TOR IV B - 25	3.71	0.03	-0.40	0.05
	TOR IV B - 35	3.98	0.02	-0.52	0.06
	TOR IV B - 45	3.58	0.03	-0.80	0.04
	TOR IV B - 55	3.98	0.04	-0.53	0.05
	TOR IV B - 65	3.92	0.04	-0.22	0.04
	TOR IV B - 75	4.48	0.10	-0.64	0.09
	TOR IV B - 85	4.41	0.05	-0.44	0.04
	TOR IV B - 95	3.83	0.02	-1.15	0.04
	TOR IV B - 105	4.03	0.03	-1.19	0.03

	TOR IV B - 115	4.31	0.08	-0.87	0.08
	TOR IV B - 125	3.81	0.03	-0.75	0.04
	TOR IV B - 135	3.65	0.04	-0.93	0.03
	TOR IV B - 145	3.63	0.04	-0.66	0.04
	TOR IV B - 155	3.83	0.04	-1.09	0.03
	TOR IV B - 165	3.60	0.03	-1.09	0.03
	TOR IV B - 185	3.46	0.02	-1.67	0.04
	TOR IV B - 195	3.30	0.06	-1.80	0.04
	TOR IV B - 205	3.47	0.08	-1.74	0.04
	TOR IV C - Base	4.32	0.08	0.00	0.08
	TOR IV C - Meio	4.19	0.07	-0.10	0.06
	TOR IV C - Topo	3.63	0.04	-0.55	0.06
	TOR IV D - Mound	3.92	0.09	0.14	0.10
	TOR VI A - Base	3.98	0.03	-1.35	0.04
	TOR VI A - Meio	3.94	0.04	-1.36	0.04
	TOR VI A - Topo	3.34	0.04	-1.95	0.04
	TOR VI B - Base	4.31	0.02	-0.57	0.03
	TOR VI B - Meio	4.04	0.05	-0.78	0.04
	TOR VI B - Topo	3.83	0.02	-0.57	0.03
	TOR VII A - 0	4.12	0.08	-0.59	0.06
	TOR VII A - 10	4.04	0.02	-1.01	0.03
	TOR VII A - 20	3.79	0.06	-1.21	0.05
	TOR VII A - 30	3.89	0.03	-1.13	0.03
	TOR VII A - 40	3.98	0.05	-0.79	0.04
	TOR VII A - 50	3.62	0.03	-1.28	0.03
	TOR VII A - 60	3.74	0.03	-1.06	0.05
	TOR VII A - 70	3.52	0.03	-1.42	0.04
	TOR VII A - 80	3.68	0.04	-1.22	0.05
	TOR VII A - 90	3.48	0.04	-1.29	0.07
	TOR VII A - 100	2.44	0.09	-2.71	0.07
	TOR VII A - Mound	3.19	0.05	-0.75	0.03
Microfábricas					
Esparita	TOR IV A - mound	3.79	-	0.29	-
	TOR IV A - base	3.36	-	-0.85	-
	TOR IV D - Mound	3.68	-	0.60	-
	TOR VI B - Base	3.60	-	-1.21	-
	TOR VI B - Topo	3.51	-	0.49	-
	TOR VII A - Mound	3.81	-	0.17	-
	TOR VII A - Base	3.64	-	0.46	-
Micrita	TOR IV A - mound	3.45	-	2.32	-
	TOR IV A - base	3.49	-	1.75	-

	TOR IV D - Mound	4.54	-	1.38	-
	TOR VI B - Base	4.69	-	1.62	-
	TOR VI B - Meio	3.84	-	0.33	-
	TOR VI B - Topo	3.78	-	1.62	-
	TOR VII A - Mound	3.19	-	1.72	-
	TOR VII A - Base	3.02	-	1.37	-
Micrita em clots	TOR IV A - meio	4.09	-	0.03	-
	TOR IV B - Meio	4.02	-	0.14	-
	TOR VI B - Meio	4.14	-	0.36	-
Tufa	TOR IV B - Topo	2.16	-	-2.43	-
	TOR IV C - Topo	1.78	-	-2.51	-
	TOR VII A - Topo	1.55	-	-1.73	-

APÊNDICE 5 – DIAGRAMAS DE VARIAÇÃO $\Delta^{13}C$ E $\Delta^{18}O$, RESPECTIVAS CORRELAÇÕES DRX E PETRO

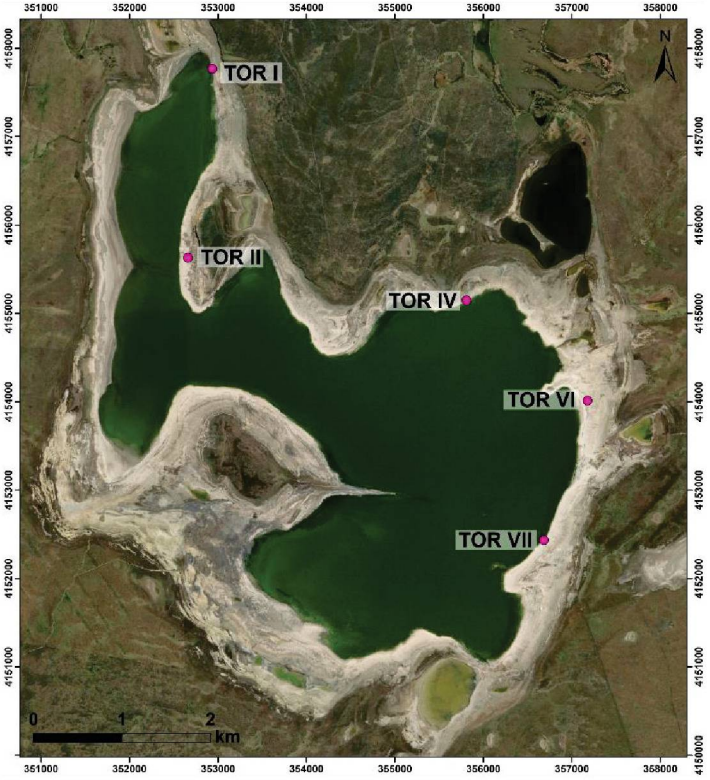

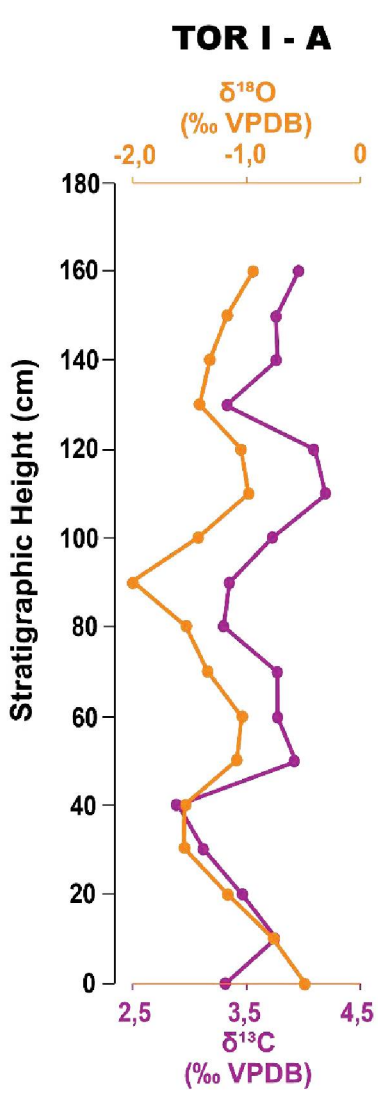

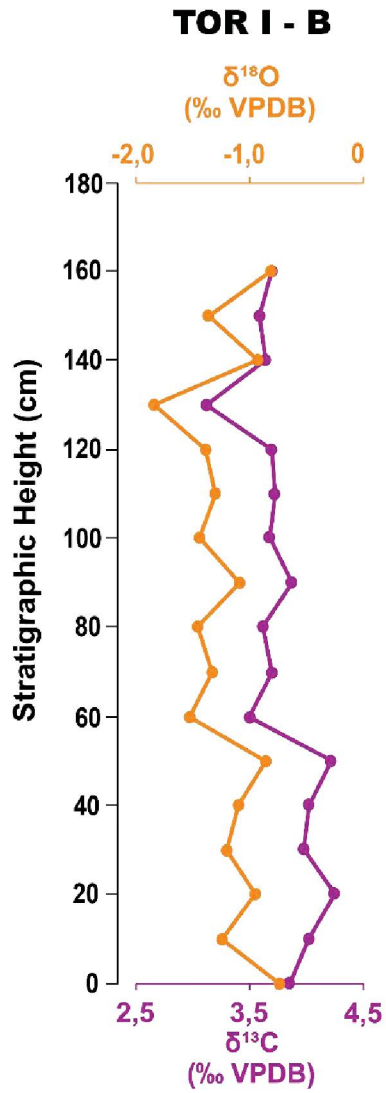

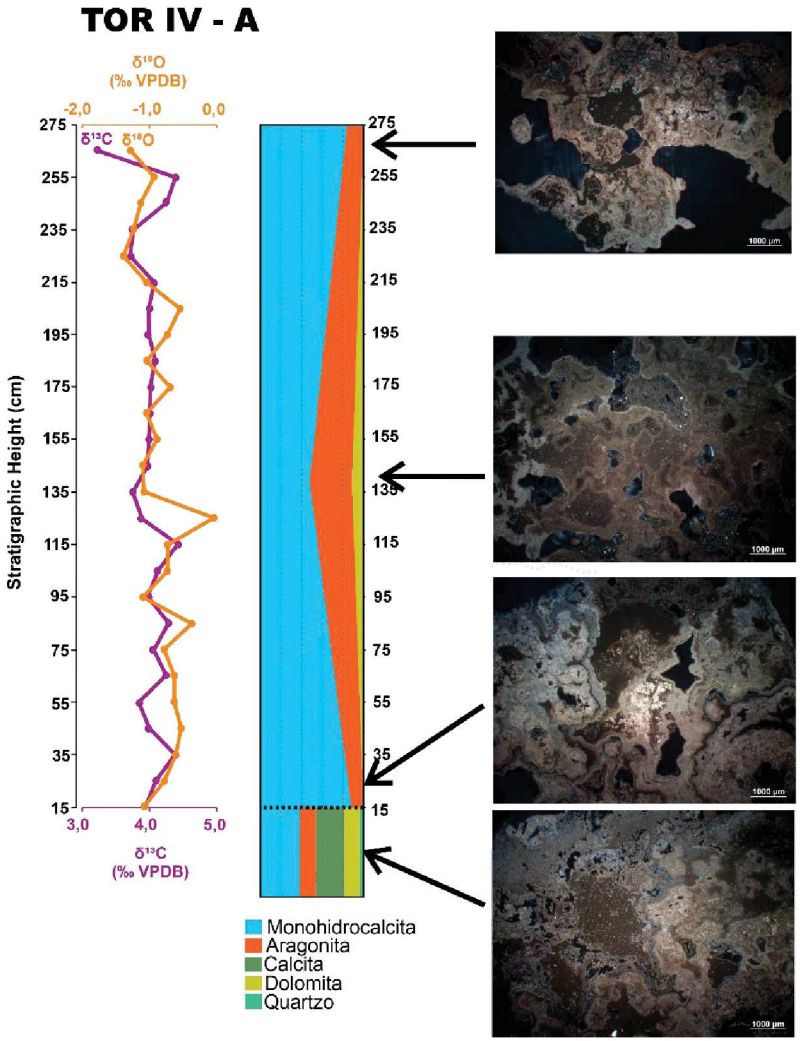
TOR IV - A
δ18O
(‰ VPDB)
-2,0
-1,0
0,0
δ13C δ18O
Stratigraphic Height (cm)
275
255
235
215
195
175
155
135
115
95
75
55
35
15
3,0
4,0
5,0
δ13C
(‰ VPDB)
Monohidrocalcita
Aragonita
Calcita
Dolomita
Quartzo
1000 µm

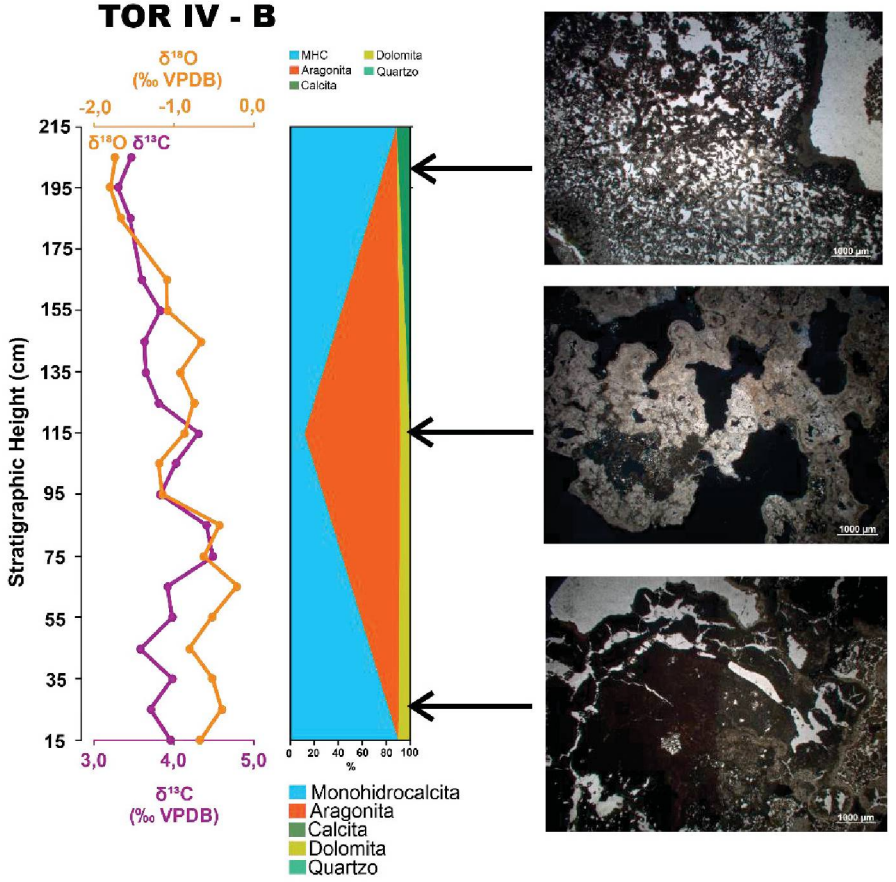
TOR IV - B
δ18O
(‰ VPDB)
-2,0
-1,0
0,0
δ18O δ13C
MHC
Dolomita
Aragonita
Quartzo
Calcita
Stratigraphic Height (cm)
215
195
175
155
135
115
95
75
55
35
15
3,0
4,0
5,0
δ13C
(‰ VPDB)
0
20
40
60
80
100
%
Monohidrocalcita
Aragonita
Calcita
Dolomita
Quartzo
1000 µm

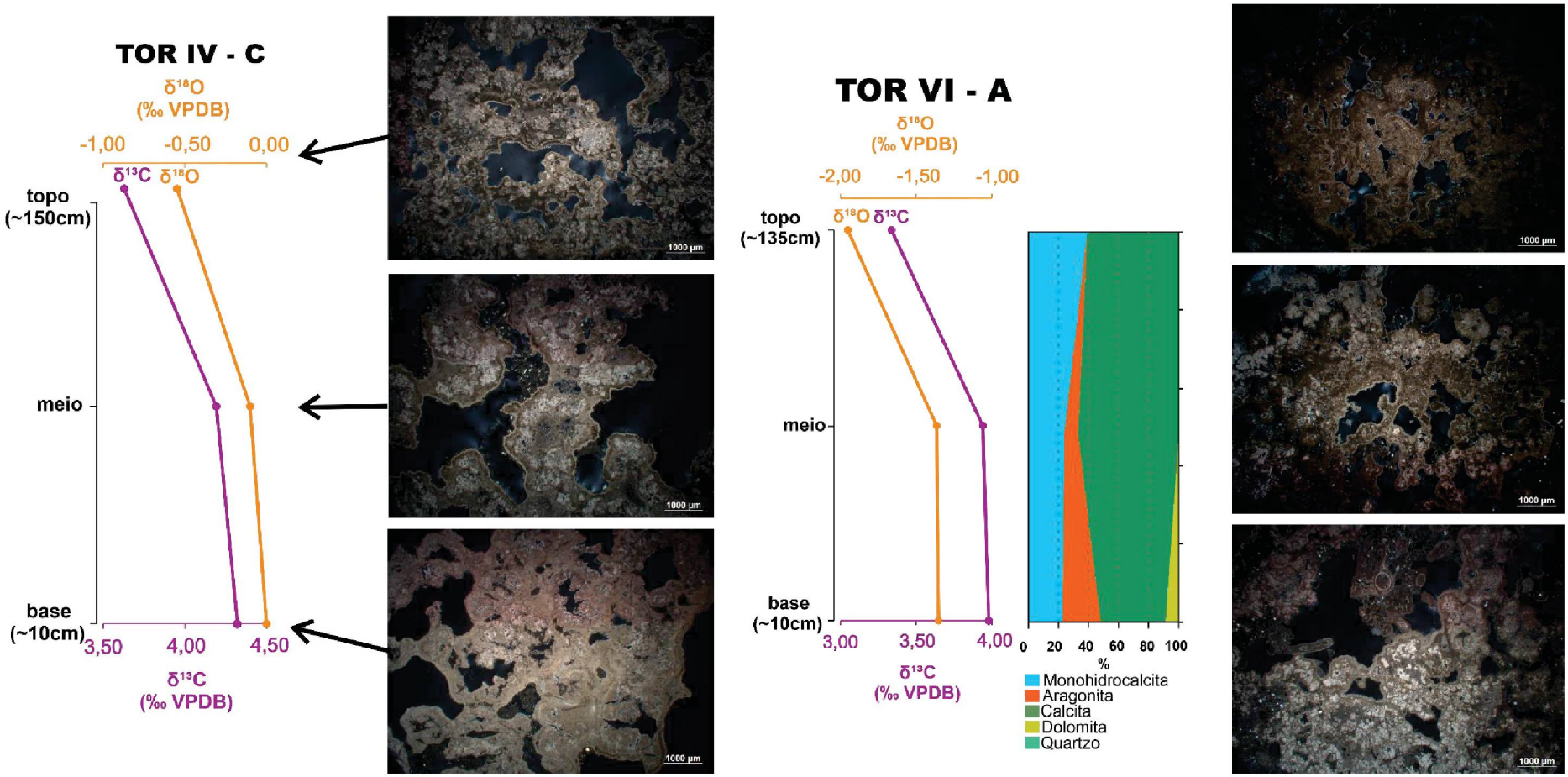
TOR IV - C
δ18O
(‰ VPDB)
-1,00
-0,50
0,00
δ13C δ18O
topo
(~150cm)
meio
base
(~10cm)
3,50
4,00
4,50
δ13C
(‰ VPDB)
1000 µm
1000 µm
1000 µm
TOR VI - A
δ18O
(‰ VPDB)
-2,00
-1,50
-1,00
topo
(~135cm)
δ18O δ13C
meio
base
(~10cm)
3,00
3,50
4,00
δ13C
(‰ VPDB)
0
20
40
60
80
100
%
Monohidrocalcita
Aragonita
Calcita
Dolomita
Quartzo
1000 µm
1000 µm
1000 µm

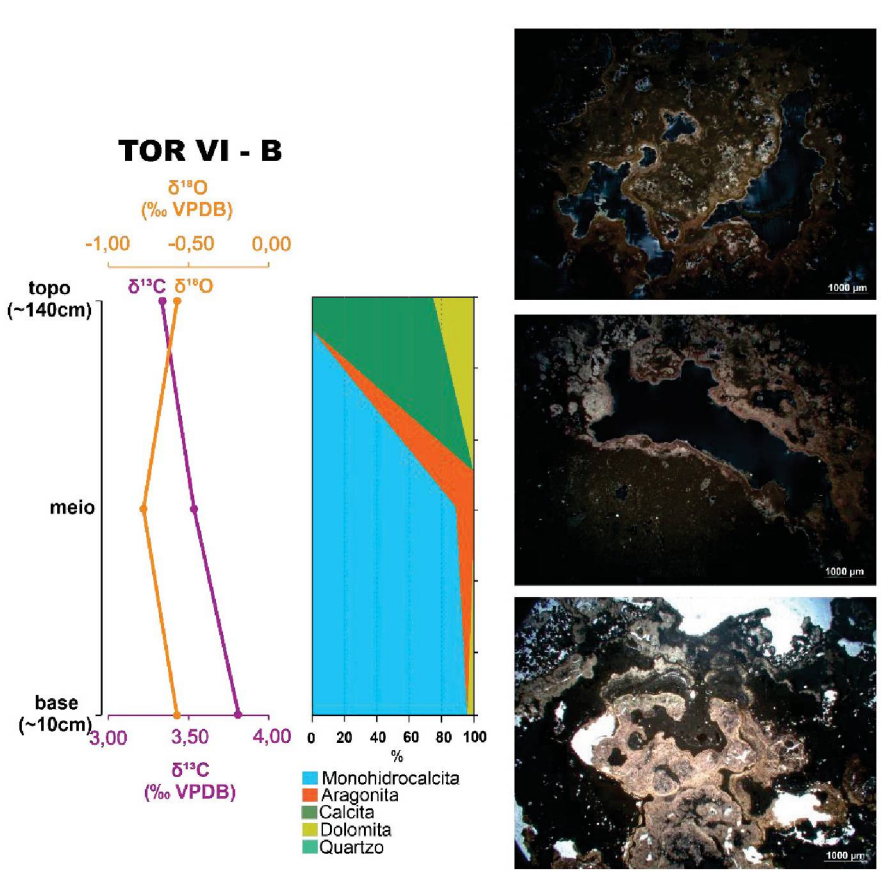
TOR VI - B
δ18O
(‰ VPDB)
-1,00
-0,50
0,00
topo
(~140cm)
δ13C δ18O
meio
base
(~10cm)
3,00
3,50
4,00
δ13C
(‰ VPDB)
0 20 40 60 80 100
%
Monohidrocalcita
Aragonita
Calcita
Dolomita
Quartzo
1000 µm
1000 µm
1000 µm

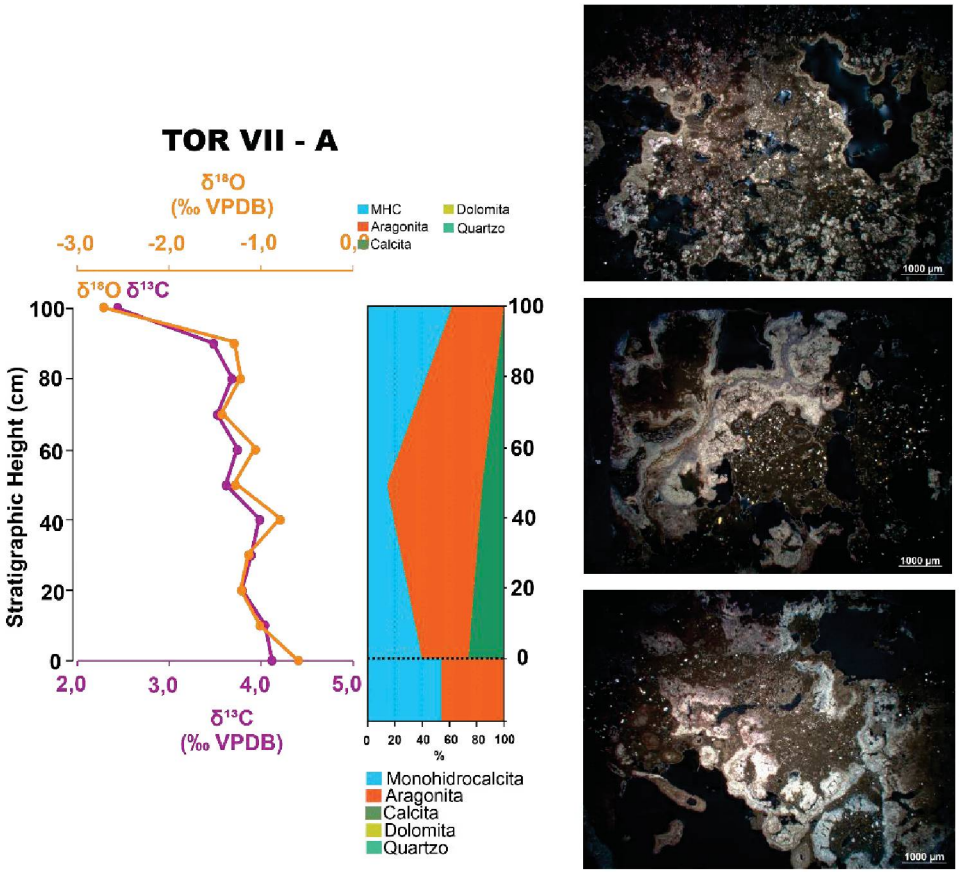
TOR VII - A
δ18O
(‰ VPDB)
-3,0
-2,0
-1,0
0,0
MHC
Aragonita
Calcita
Dolomita
Quartzo
δ18O δ13C
Stratigraphic Height (cm)
100
80
60
40
20
0
2,0
3,0
4,0
5,0
δ13C
(‰ VPDB)
0 20 40 60 80 100
%
Monohidrocalcita
Aragonita
Calcita
Dolomita
Quartzo
1000 µm
1000 µm
1000 µm